AD-A194 690 A STUDY OF IMPURITIES IN COMBUSTION SYNTHESIS SYSTEMS 1/1
(U) ARMY BALLISTIC RESEARCH LAB ABERDEEN PROVING GROUND
MD L J KECSKES ET AL APR 88 BRL-MR-3658

UNCLASSIFIED F/G 11/2 NL

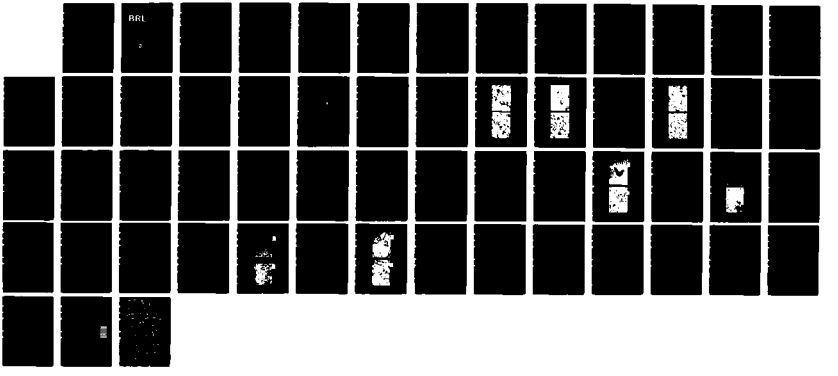

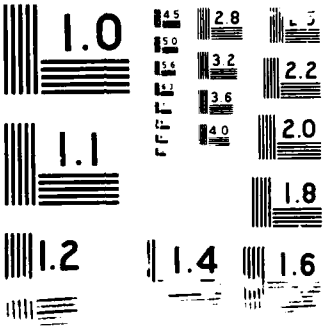
1.0
1.1
1.2
1.4
1.6
1.8
2.0
2.2
2.8
3.2
3.6
4.0
4.5
5.0

MEMORANDUM REPORT BRL-MR-3658

BRL

1938 – Serving the Army for Fifty Years – 1988

A STUDY OF IMPURITIES IN COMBUSTION SYNTHESIS SYSTEMS

LASZLO J. KECSKES
ANDRUS NIILER

APRIL 1988

U.S. ARMY LABORATORY COMMAND

BALLISTIC RESEARCH LABORATORY
ABERDEEN PROVING GROUND, MARYLAND

DESTRUCTION NOTICE

Destroy this report when it is no longer needed. DO NOT return it to the originator.

Additional copies of this report may be obtained from the National Technical Information Service, U.S. Department of Commerce, Springfield, VA 22161.

The findings of this report are not to be construed as an official Department of the Army position, unless so designated by other authorized documents.

The use of trade names or manufacturers' names in this report does not constitute indorsement of any commercial product.

UNCLASSIFIED
SECURITY CLASSIFICATION OF THIS PAGE

ADA194690

REPORT DOCUMENTATION PAGE

Form Approved
OMB No. 0704-0188

1a. REPORT SECURITY CLASSIFICATION Unclassified	1b. RESTRICTIVE MARKINGS
2a. SECURITY CLASSIFICATION AUTHORITY N/A	3. DISTRIBUTION / AVAILABILITY OF REPORT
2b. DECLASSIFICATION / DOWNGRADING SCHEDULE N/A	
4. PERFORMING ORGANIZATION REPORT NUMBER(S) BRL-MR-3658	5. MONITORING ORGANIZATION REPORT NUMBER(S)
6a. NAME OF PERFORMING ORGANIZATION US Army Ballistic Research Laboratory 6b. OFFICE SYMBOL (*If applicable*) SLCBR-TB	7a. NAME OF MONITORING ORGANIZATION
6c. ADDRESS (*City, State, and ZIP Code*) Aberdeen Proving Ground, Maryland 21005-5066	7b. ADDRESS (*City, State, and ZIP Code*)
8a. NAME OF FUNDING / SPONSORING ORGANIZATION US Army Ballistic Research Laboratory 8b. OFFICE SYMBOL (*If applicable*) SLCBR-D	9. PROCUREMENT INSTRUMENT IDENTIFICATION NUMBER
8c. ADDRESS (*City, State, and ZIP Code*) Aberdeen Proving Ground, Maryland 21005-5066	10. SOURCE OF FUNDING NUMBERS PROGRAM ELEMENT NO. / PROJECT NO. / TASK NO. / WORK UNIT ACCESSION NO.

11. TITLE (*Include Security Classification*)
(U) A Study of Impurities in Combustion Synthesis Systems

12. PERSONAL AUTHOR(S)
Laszlo J. Kecskes and Andrus Niiler

13a. TYPE OF REPORT	13b. TIME COVERED	14. DATE OF REPORT (*Year, Month, Day*)	15. PAGE COUNT
MR	FROM _____ TO _____		

16. SUPPLEMENTARY NOTATION

17. COSATI CODES			18. SUBJECT TERMS (*Continue on reverse if necessary and identify by block number*).
FIELD	GROUP	SUB-GROUP	
11	02		

19. ABSTRACT (*Continue on reverse if necessary and identify by block number*) (weh)

This investigation is directed toward a detailed understanding of the nature of the evolution of solid and gaseous impurities during the Combustion Synthesis (Self-Propagating High Temperature Synthesis) of ceramic materials. The identities and amounts of the volatile impurities present on various reactant powders were measured and the effects of storage and handling conditions evaluated using a vacuum furnace and a Residual Gas Analyzer. The extent to which these impurities volatilize, react with each other, and affect the reaction dynamics and product structure were analyzed for the titanium+carbon system. The result indicate that the major volatile impurity species on the reactant powders are water vapor, hydrogen, carbon monoxide, carbon dioxide, and hydrocarbons. Further Residual Gas Analysis, Scanning Electron Microscopy, and Ion Beam Analyses reveal marked differences in both non-condensible and condensible impurity species evolved by the reacting Ti+C system. It is found that the physical and mechanical properties of the ceramic material will be significantly improved if the impurities are eliminated with a 500C vacuum bakeout.

20. DISTRIBUTION / AVAILABILITY OF ABSTRACT	21. ABSTRACT SECURITY CLASSIFICATION
☒ UNCLASSIFIED/UNLIMITED ☒ SAME AS RPT ☐ DTIC USERS	UNCLASSIFIED
22a. NAME OF RESPONSIBLE INDIVIDUAL Laszlo J. Kecskes	22b TELEPHONE (*Include Area Code*) 301/278-2557
	22c. OFFICE SYMBOL SCLBR-TB-E

DD Form 1473, JUN 86 *Previous editions are obsolete.*

SECURITY CLASSIFICATION OF THIS PAGE
UNCLASSIFIED

TABLE OF CONTENTS

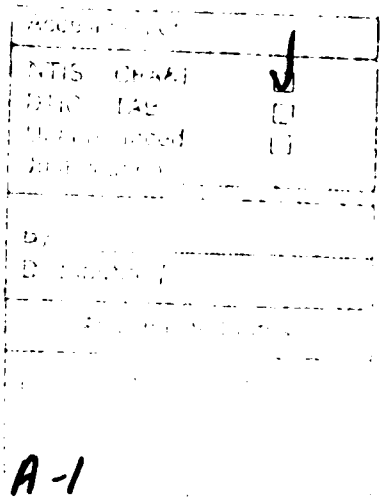

A-1

LIST OF FIGURES

LIST OF TABLES

1. INTRODUCTION

Self-Propagating High-Temperature Synthesis (SHS) is a process by which a variety of ceramics and cermets can be produced directly from the constituent powders. Originally developed in the Soviet Union, SHS has also been studied extensively in the United States during the past decade. An excellent compilation of much of the Soviet literature can be found in Ref. 1. A general review of the most recent US work in SHS is given in the proceedings of the ARMY/Defense Advanced Research Projects Agency (DARPA) Symposium on SHS,[2] a summary of which appears in Ref. 3.

SHS is a solid combustion process characterized by an exothermic heat release sufficient to propagate a combustion front through the powder compact, completely consuming the reactant powders once ignition is achieved. These SHS reactions occur at temperatures in excess of 2000C, a temperature which is high enough to cause the evolution of most impurities that may be found on the reactants. Although this evolution of the impurities is good in the sense that the final product is left with a much lower impurity content than was present in the starting materials, the high reaction temperatures sometimes cause the evolution of these impurities to be violent. The consequences of this violent gas evolution are the formation of gas channels, voids, and open cracks in the reacted ceramic body[4,5], and in some instances, even a complete disruption of the reaction resulting in the powder compact being blown apart. However, when the reactant powders have been vacuum baked at 400C to 500C or high purity powders are used, the amount of evolved gases is much reduced and the integrity of the product is improved.

A large variation in the amount of impurities has been observed on commerical titanium and carbon powders. There are two major reasons for these variations. The first is that the powders undergo significantly different fabrication procedures from the raw materials used, to the actual processing conditions, to post processing treatments. The second reason arises from different storage, shipment, and handling conditions. The first reason not only explains the variations in the impurity levels, but also accounts for considerably different powder morphology. The powder morphology, i.e. size, shape and surface area, in turn strongly affect the amounts and types of impurities that can be picked up by that powder subsequent to fabrication.

An example of the type of impurities that can be incorporated into titanium powder in fabrication is illustrated in the following description of the Kroll process.[6,7] In this process Ti powder can be produced by reducing titanium tetrachloride in the presence of melted magnesium. When the reaction is complete, the titanium metal is included in a solidified mass along with magnesium, magnesium chloride, and titanium subchlorides. A hydrochloric acid leach is used to remove all but the titanium metal which is left in a porous, spongy mass. The process continues by comminution of the sponge into powder or melting it into an ingot, both steps which may leave traces of magnesium, magnesium chloride or the oxides and nitrides of titanium. Because of the great affinity of the titanium metal for oxygen and nitrogen and difficulties in completely eliminating all water vapor, the powder crushing step can result in large amounts of oxide and nitride layers on the powders.

In addition to the problems caused by the fabrication techniques, the investigation of the presence of impurities must also consider the powders' history, i.e., what sort of environment that particular batch was subjected to during storage, shipment and handling in the laboratory. Powders of the size to be of interest here will readily absorb large quantities of water vapor in a few days, once exposed to even relatively dry air (30-40% RH). The chemical and physical surface activities of a metal powder determine how readily it will adsorb volatiles onto its surface and allow their diffusion into the particle's interior. For example, while some metal powders such as aluminum will form a passivating oxide coating that prevents further degradation of the powder, titanium will break down the water molecule and form a thick but permeable oxide coating on the surface that will allow additional water vapor to diffuse into the powder particle's interior. Over a period of time, the powder can gain oxygen and hydrogen from the water vapor in the air. In sufficient concentrations, the oxygen and hydrogen form compounds both at the surface and in the interior of the titanium powder. However, unlike the reversible absorption of hydrogen, the absorption of oxygen is irreversible.[8] The desorption of trapped chemical species from the surface and interior is controlled by the chemical attraction between the adsorbate ions and the powder material and depends little on particle morphology. That is, in many cases the chemical bond between the powder particle surface and the adsorbate ions is greater than the attraction of the free and unbound adsorbate species to itself.

This investigation of volatiles present on reactant powders as well as their evolution during SHS reactions has been carried out in two parts. In the first, the objective was to determine in detail the identities and amounts of the volatile impurities that are present on the reactant powders as received from vendors and how various storage and handling conditions affect these impurities. In this phase of the experimentation, a vacuum furnace was used to bake small amounts of the powders and, as they were driven off, the non-condensing, volatile species were measured with a Residual Gas Analyzer. The second objective was to determine the extent to which the impurities present on the powders volatilize, react with each other, or with the powders themselves during the synthesis reaction and the effect that these escaping volatiles have on the reaction dynamics as well as the product structure. This was accomplished by measuring both non-condensible and condensible species given off by the reacting titanium-carbon system. The morphologies of reactant powder particles as well as the reacted products were examined with the aid of Scanning Electron Microscopy. The condensibles were examined with Rutherford Backscattering and proton induced X-Ray methods.

2. EXPERIMENTAL TECHNIQUE

The powders studied in this investigation are listed in Table 1 along with pertinent information about each. The part that each had in the experiments is identified in the section where that particular measurement is described.

2.1 Reactant Bakeout Measurements. The schematic diagram of the vacuum bakeout apparatus is shown in Fig. 1. The oven is a manually operated, single zone, 5.1 cm ID, Lindberg tube furnace capable of temperatures from 200C to 1200C. A 2.2 cm Vycor combustion tube is connected to a vacuum manifold

designed to be easily disassembled for maintenance. The system is pumped by a liquid nitrogen baffled oil diffusion pump capable of a system pressure of 10^{-6} torr. A small amount of powder, about 1g, is loaded into a combustion boat and inserted into the tube furnace. The furnace temperature is set and allowed to soak while the gas species are released from the powders. Figure 2 shows a typical Residual Gas Analyzer (RGA) spectrum of ion current vs. mass/charge (m/q) for the CA graphite taken at 200C. In this example, the peaks due to atomic hydrogen, carbon, water, carbon monoxide, and carbon dioxide from the powder and system background are seen. This particular scan is taken 15 minutes after the furnace reached the set temperature of 200C. Integrating the peaks shown in this spectrum results in the type of data shown in Fig. 3 where the time history of the evolution of hydrogen (at m/q=2), water vapor (at m/q=18), and carbon dioxide (at m/q=44) with the furnace at 200C are shown. RGA scans at each set temperature are taken at intervals of about 6 minutes until all the partial pressures of the released gases reach asymptotic, equilibrium levels.

TABLE 1

Description of Powders

DESIGNATION	SIZE MESH	PURITY [%]	DESCRIPTION	MANUFACTURER
AE Ti	-325	99.7	Titanium	Atlantic *
CA Ti	-325	99.0	Titanium	ConAstro **
CA Ti2	-400	99.0	Lot 1086 Titanium	ConAstro **
MON C	.05μm	98.0	Monarch 1100 Carbon 98% fixed C content	Cabot ***
CA Gr	-325	99+	Lot 412 Oxidation Resistant Graphite	ConAstro **
CE Gr	-325	99.9	Lot 5405 Graphite	Cerac ****
CA Bc	-325	99.5	Lot 105 Crystalline Boron	ConAstro **
CA Ba	5.0μm	96.0	Lot 110 Amorphous Boron	ConAstro **

* Atlantic Equipment Engineers, Bergenfield, NJ.

** Consolidated Astronautics Inc., Long Island City, NY.

*** Cabot Corp., Boston, MA.

**** CERAC, Inc., Milwaukee, WI.

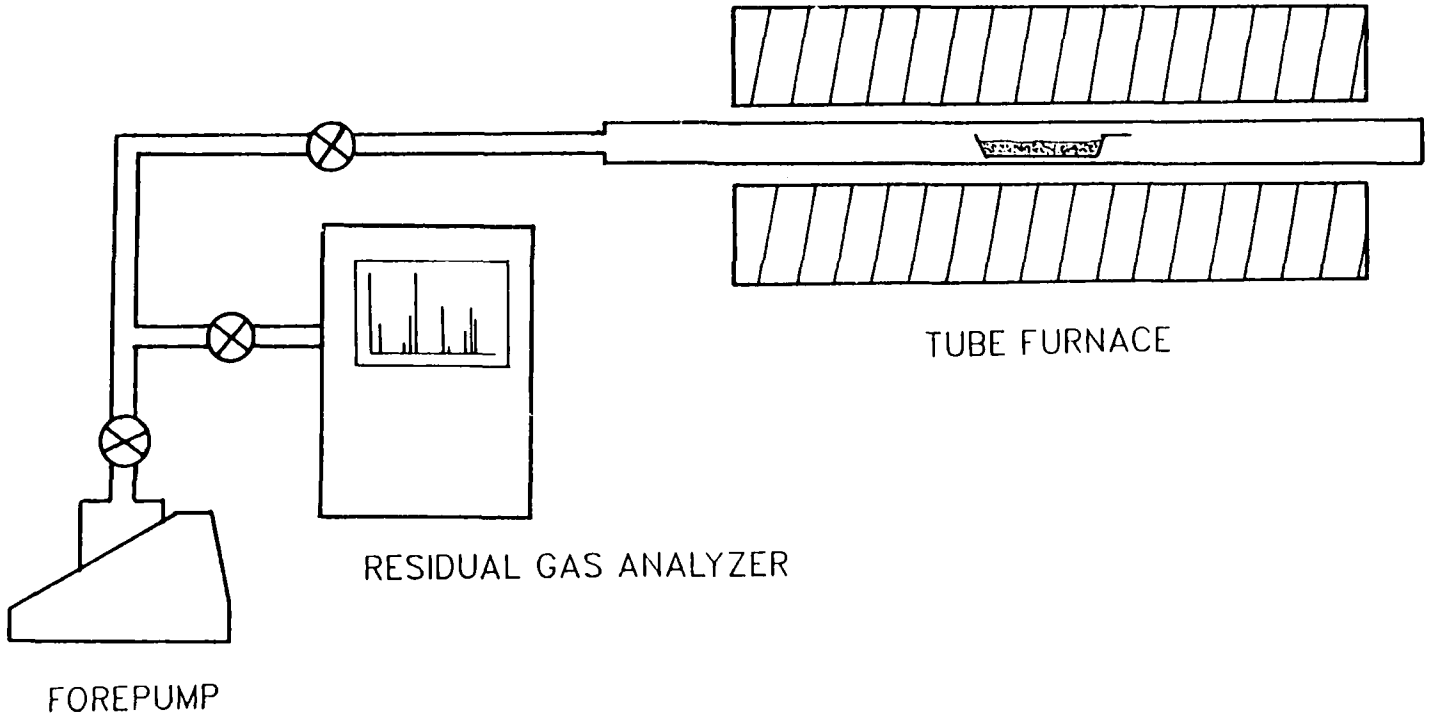

Figure 1. Schematic diagram of bakeout apparatus showing furnace with inserted powder sample, Residual Gas Analyzer, and pumping system.

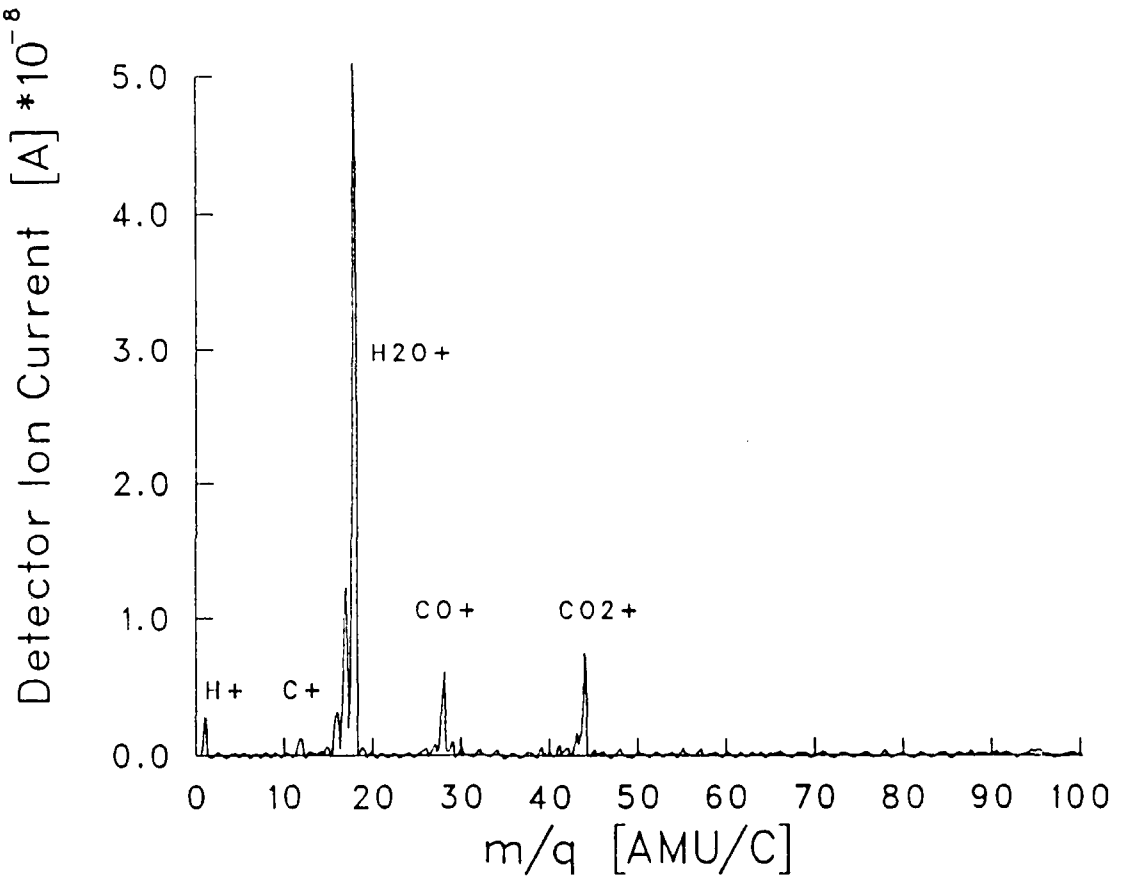

Figure 2. Residual Gas Analyzer Spectrum for -325 mesh CA Graphite. The scan taken 15 minutes after the oven reached the set temperature shows peaks due to atomic hydrogen, carbon, water vapor, carbon monoxide, and carbon dioxide.

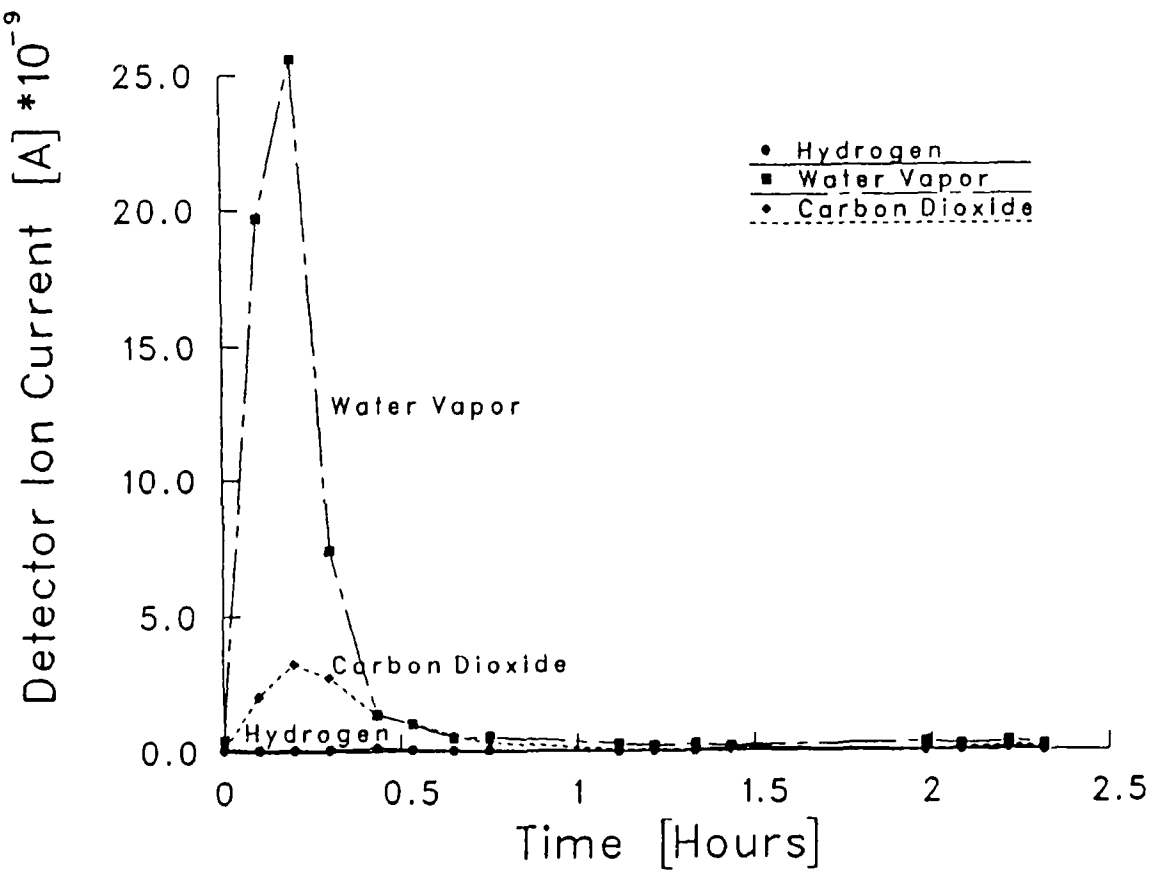

Figure 3. Time evolution of molecular hydrogen (m/q=2), water vapor (m/q=18), and carbon dioxide (m/q=44) at 200C from CA Graphite powder shown in Figure 2. The lines are drawn to guide the eye.

The area under the curves shown in Fig. 3 represents the amount of a given species which is baked out at that given temperature. The plot of these areas against temperature reveals the minimum temperature (i.e. the temperature at which a given species is no longer evolved) necessary to drive off a particular impurity. The temperature profiles of water and hydrogen for the CA graphite and AE titanium powders are shown in Fig. 4 and Fig. 5. Since the lowest temperature setting of the tube furnace is 200C, some of the water peak at 200C in Fig. 4 may have evolved at a much lower temperature. Note the fact that there is very little molecular hydrogen in the CA graphite com-pared to AE titanium. Figure 6 shows similar temperature profiles for the evolution of carbon dioxide and carbon monoxide from the CA graphite. Data similar to what is shown in Figs. 4, 5 and 6 were obtained for other species also, with the results being discussed later.

A careful species analysis while vacuum baking was done on most of the powders. In addition a crude thermogravimetric analysis was done on some of the other powders. The total mass loss experienced by the small powder samples while they were being baked was measured. These results will also be discussed later.

2.2 Non-condensible Impurities from the SHS Reaction. The schematic diagram of the reaction chamber used in the second set of experiments is shown in Fig. 7. The reaction chamber had a volume of 5.07 liters and was pumped by a turbomolecular pump capable of a base pressure in the system of about 10^{-4} torr. A tungsten filament, attached through vacuum feedthroughs to a high current DC power supply, was used both to heat samples during baking procedure and to ignite the SHS reaction in the sample. A digital capacitance manometer was used to measure pressures in the 10^{-3} to 10^{+2} torr range. A removable side chamber of well known volume, 0.33 liters, was attached to the reaction chamber, separated by a valve, for the purpose of collecting the volatile gases given off during a reaction.

Green compacts were made from stoichiometric mixtures of as received AE titanium and CA graphite powders. The powders were mixed in a ball mill for 1 hour and stored in a sealed container under argon. The compacts were uniaxially pressed to 0.27 GPa in a 0.6 cm cylindrical die. Upon extraction from the die, the compacts were weighed and stored in a sealed plastic bottle under argon. The Ti+C compact was placed in the reaction chamber and pumped down to a base pressure of at least 10^{-4} torr. Prior to ignition, the gate valve was closed and the reaction and gas collection chambers were filled with argon to a pressure of 1 torr. This known amount of argon in the collection chamber, n, (from the ideal gas law PV=nRT), was used to provide an absolute standard against which the reaction gas volumes were later measured in the RGA. In a typical experiment where a 1.0g (1.5×10^{-2} moles) Ti+C sample was reacted, the total pressure reached by the the two chamber volumes was about 8 torr which is equivalent to about 3.1×10^{-3} moles of gas at room temperature.

The reaction chamber was a 10.0 cm ID stainless steel cross with a viewing port and a number of feedthroughs, valves and gauges attached at various locations. Due to this complicated geometry, its volume could not be determined by simple dimension measurements. On the other hand, the collection

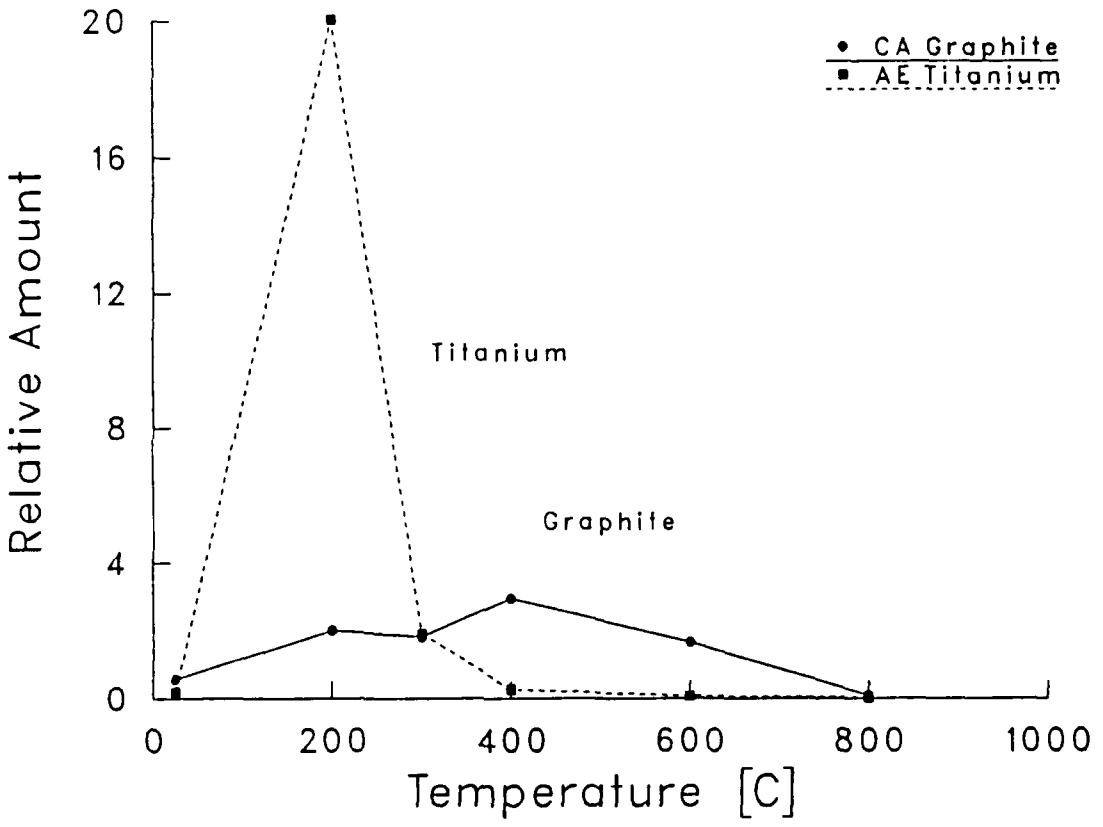

Figure 4. Temperature dependence of water vapor evolution from CA Graphite and AE Titanium powders. The lines are drawn to guide the eye.

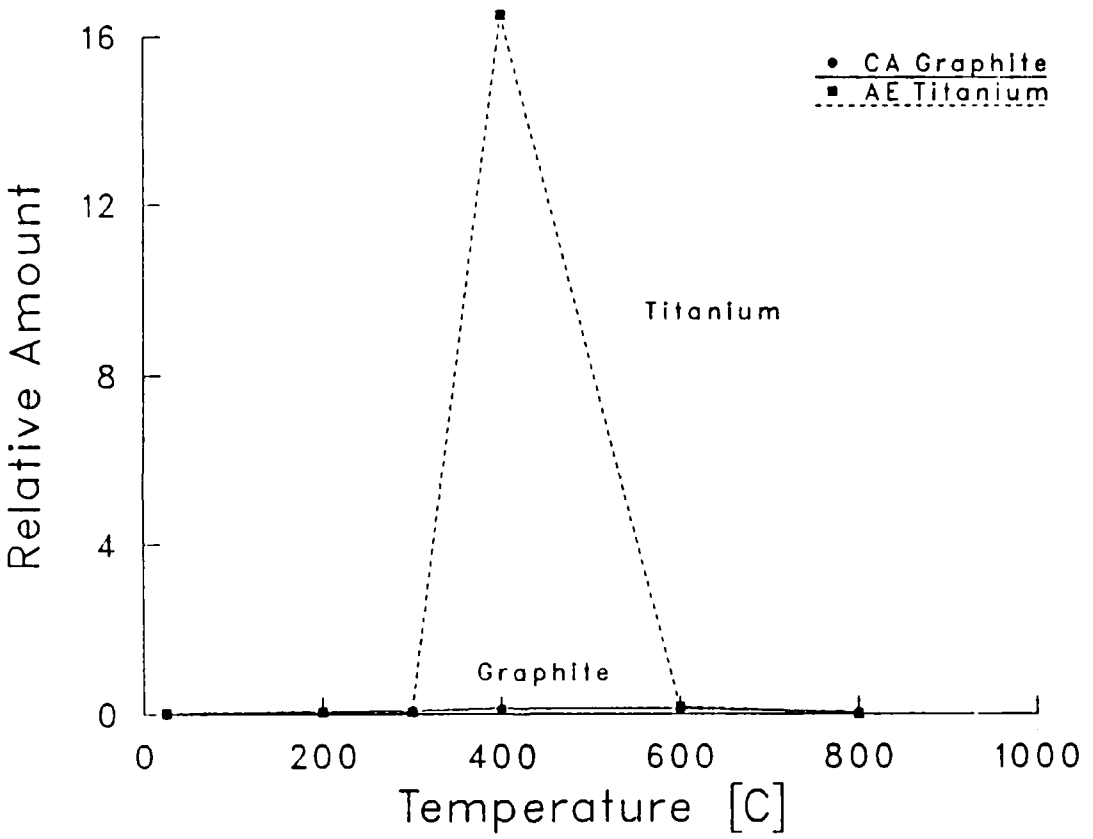

Figure 5. Temperature dependence of molecular hydrogen evolution from CA Graphite and AE Titanium powders. Note the small quantities of H_2 on the graphite. The lines are drawn to guide the eye.

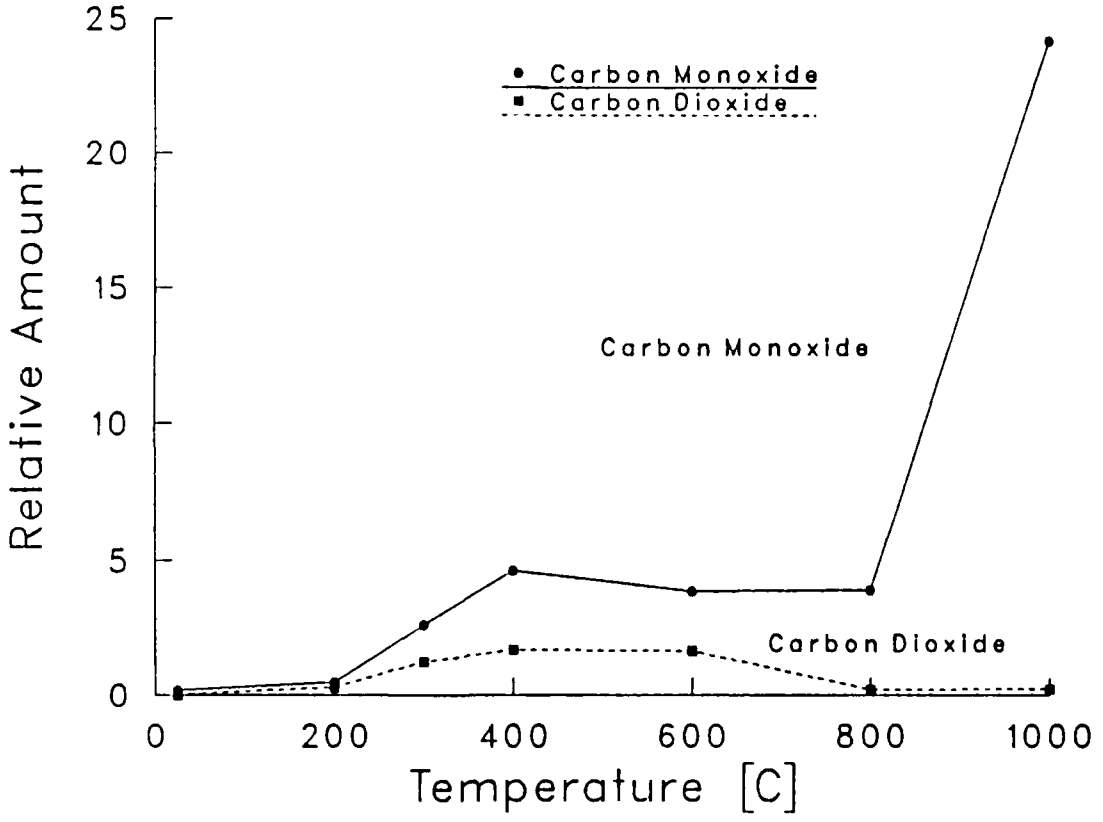

Figure 6. Temperature dependence of carbon dioxide and carbon monoxide evolution from CA Graphite. The lines are drawn to guide the eye.

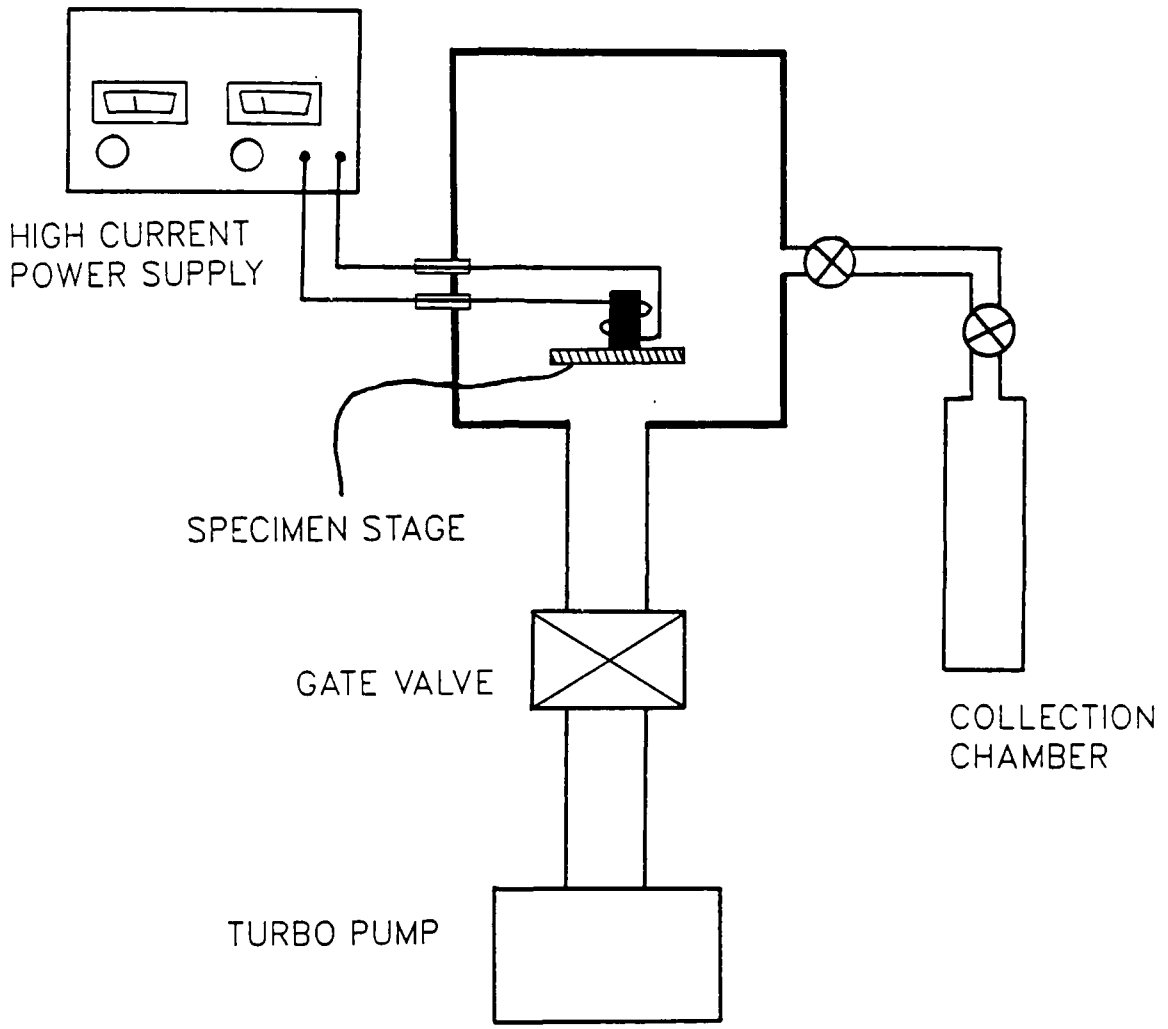

Figure 7. Schematic diagram of reaction chamber, showing specimen, ignition system, collection chamber, and vacuum system.

chamber was made of three copper tube sections, making its volume easily and accurately determinable. Consequently, the following procedure was used in determining the volume of the reaction cham er. The whole system, including the collection chamber, was pumped to the base pressure of 10^{-4} torr. The valve to the pump was closed off and the whole system was backfilled with argon to a pressure of 8.77 torr. The collection chamber was closed off and the rest of the system again pumped down to 10^{-3} torr. The pump valve was then closed and the collection bottle valve opened, releasing the argon trapped therein to the rest of the system. The familiar relationship, $PV/T = P'V'/T'$, can now be used, where the unprimed quantities refer to the collection chamber alone and the primed quantities refer to the whole system. Since the temperatures remain unchanged, the volumes scale inversely with the pressures. Thus the measurement of the reaction chamber volume becomes a very simple measurement of two pressures, which was done with the capacitance manometer to better than .1%. The volumes of the collection chamber and reaction chamber were measured with an accuracy of 2%.

Two separate experiments to measure the non-condensibles were carried out with this reaction chamber. In the first, the compact was placed in the chamber, the tungsten filament was switched on to full power and the sample ignited within 10 seconds. The total energy input required to ignite the compact was roughly 15 kJ. In all cases when this sudden heating took place, the impurity gas flow was so violent that the sample was blown apart without reacting completely. In the second experiment, the sample was first outgassed with slow heating by running the filament at a low heat for ten minutes. The energy input in this part of the experiment was roughly 100 kJ. The sample was then allowed to cool down to room temperature and, after the argon fill, it was ignited with a more gradual heating of the filament. This, more gentle procedure resulted in the whole sample reacting and staying together in a single, if porous, piece. The energy required to ignite the compact in this way was about twice that of the immediate ignition, or 35 kJ. During both experiments, the evolved gases filled both the reaction and the collection chambers. After the reaction, the collection chamber was attached to the RGA and the non-condensed gases analyzed.

2.3 Condensible Impurities from the SHS Reaction. Usually, as the SHS reaction traverses a TiC green compact, a prominent, bright, yellow-green flame can be seen emanating from the sample at the reaction front. While the composition of the flame itself is probably volatilized impurities released from the reactants, the flame also carries with it a grey-black solid residue. This ejected solid residue was collected on several aluminum strips placed 3-4 cm away from the sample undergoing the SHS reaction. The aluminum targets were polished with 4000 grit paper, cleaned in Freon, and inserted into the reaction chamber. These experiments were performed with the gate valve open so that the reaction chamber pressure could be kept at a base pressure of 10^{-4} torr.

Again, two separate experiments to measure the condensibles were carried out in the reaction chamber. In the first experiment, the green compact was ignited without outgasing, as described in the previous section. In the second, the green compact was first outgassed for about 30 minutes. After allowing the compact to cool in vacuum, its weight loss was measured and the

compact reinserted into the chamber. The chamber was then again pumped to 10^{-4} torr and the reaction initiated. In the course of these experiments, two sets of condensate targets were collected: the first during the reaction of the unbaked specimen, the second during the reaction of the baked specimen.

The condensate morphology and the interior microstructure and fracture characteristics of the TiC reaction products were examined with Scanning Electron Microscopy (SEM). In addition, three different Ion Beam Analysis methods were used on the coatings produced by the SHS reactions on the baked and unbaked samples. The first was Proton Induced X-Ray Excitation (PIXE), a method which is capable of identifying all elements above Z=13 (Al). Briefly, a 1.5MeV proton beam is used to excite characteristic x-rays in the outer 10 microns of the sample surface and, after the x-rays have passed through a thin mylar foil out of the vacuum chamber, they are detected by a SiLi detector and energy analyzed and stored in a multichannel analyzer. The apparatus, however, was not calibrated for quantitative elemental concentrations. A second method was Rutherford Backscattering (RBS) with a 1.0 MeV deuteron beam. This method is highly quantitative in terms of the amount of a given element on the sample surface but since its identification of elements depends on their masses, elements which are close to each other and heavy (A>40) cannot be unambiguously identified in all cases. Depth profiling with approximately 20-30 nm resolution is also possible with RBS, a feature which, as will be seen, reveals some interesting details about the structure of the coatings. The third method which was used, also with 1.0 MeV deuterons, was Nuclear Reaction Spectroscopy, NRS. NRS is very useful for identifying the elements carbon, nitrogen and oxygen, something which is typically difficult to do with RBS. This particular capability is very important in this experiment where TiC and TiO_2 are present. A detailed description of the RBS and NRS techniques, along with the computer code PROFILE which is used to analyze the raw data, is given in Ref. 9.

3. EXPERIMENTAL RESULTS AND DISCUSSION

3.1 Starting Powder Morphologies. The morphologies of some of the powders used in this investigation were examined by Scanning Electron Microscopy. See Table 1 for a description of each of the powders. The two carbon powders are shown in Fig. 8 with MON C in 8a and CA Gr in 8b. The MON C has very small but uniform particle size of about 0.05 microns which tend to agglomerate into larger, 2 to 5 micron sized rounded particulates. The small particle size results in a large surface area for this powder so that large amounts of impurities can be absorbed by this powder. Furthermore, the impurities that absorb onto the particle surfaces will be very difficult to dislodge once they become embedded on the insides of the agglomerates. The CA Gr, -325 mesh oxidation resistant graphite, consists of about 10-20 micron platelike flakes with sharp edges. Although the graphite particles have a smaller surface area than the Monarch 1100 carbon, and thus less absorption of impurities would be expected, the extensive interplanar spacing between graphite sheets may allow for the entrapment of significant amounts of impurities.

Two of the titanium powders described in Table 1 are shown in Fig. 9, with AE Ti in 9a and CA Ti in 9b. In general, these titanium particles are somewhat larger than the carbons shown in Fig. 8 and the distributions in their shapes and sizes are also broader. The AE titanium particles tend to be

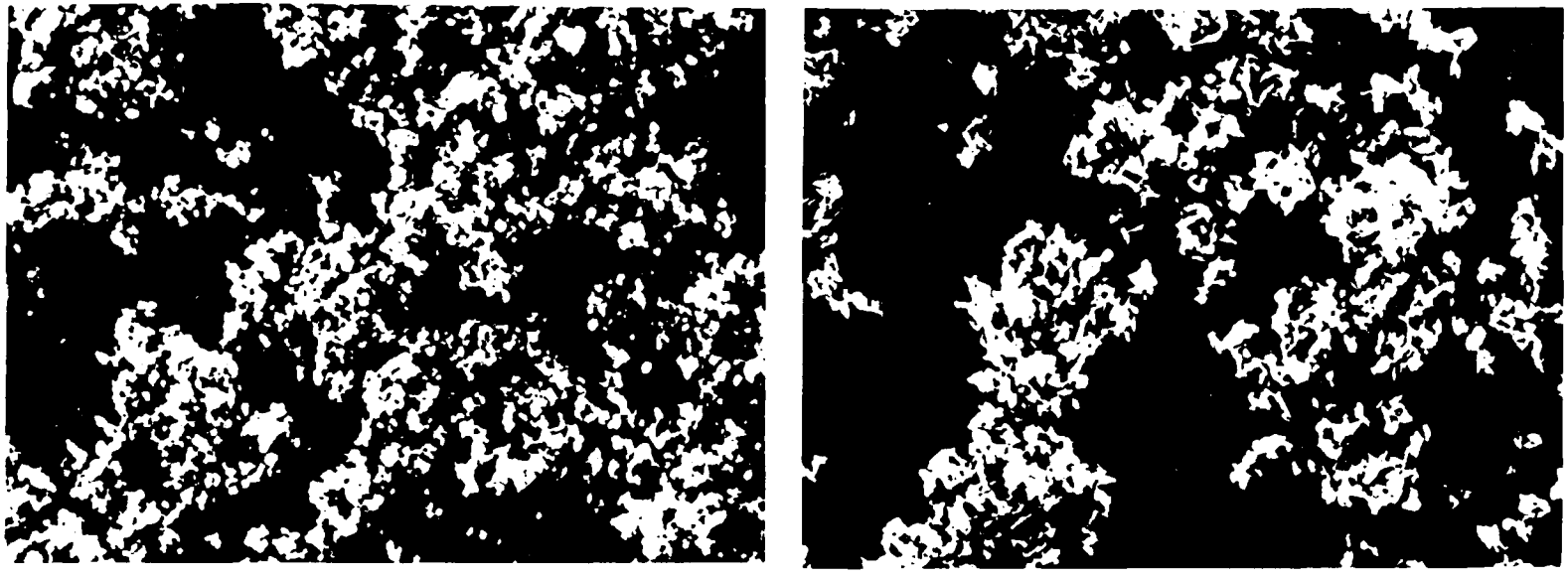

Figure 8. Scanning Electron Micrographs of the carbon starting powders with MON Carbon shown in 8a and CA Graphite in 8b. The carbon powder particles tend to be spherical while graphite tends to be flaky.

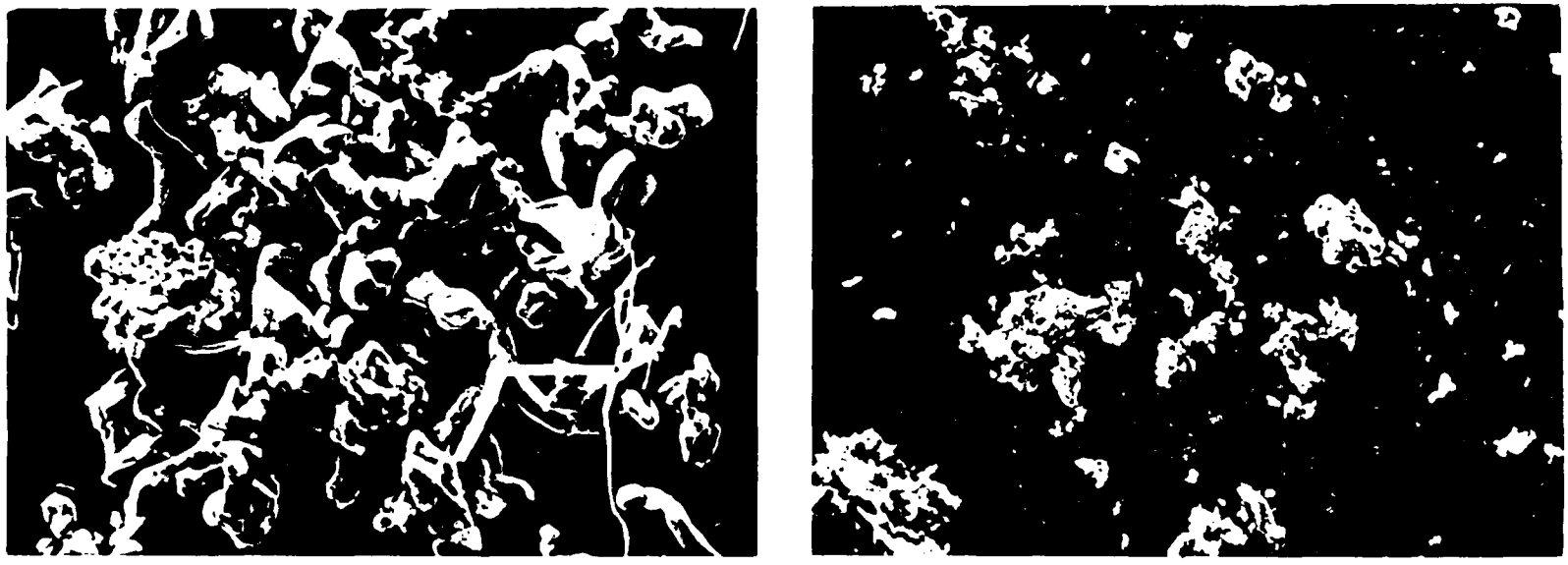

Figure 9. Scanning Electron Micrographs of the titanium starting powders with AE Ti powder shown in 9a and CA Ti powder in 9b. Although both titanium powders are -325 mesh, the particles appear to be different in both size and shape.

very large, 20-40 microns, irregularly shaped and relatively smooth on the surface. Individual particles are generally elongated, some with sharp and rounded edges. On the other hand, the CA titanium consists of an aggregate of a wide distribution of irregularly shaped, very sharp platelet-like particles ranging from a just a few microns to over 20 microns. The surfaces of individual particles also tend to be much rougher.

The morphology of the CA crystalline boron is shown in Fig. 10a and the CA amorphous boron in Fig. 10b. As can be seen, both of the borons tend to agglomerate into larger particles, probably due to the fact that boron is highly hygroscopic. The individual grains of crystalline boron have fairly sharp edges with an average particle size of about 5 microns. The amorphous boron has a similar particle shape, but the individual particles are somewhat smaller, averaging about 2 microns.

3.2 Reactant Bakeout Results. In analyzing the results of the vacuum bakeout experiment, the expression used to convert the RGA detector ion current to mole fractions of a given gaseous species, X_i, is given by

$$X_i = \frac{n_i}{\Sigma n_i} \quad . \tag{1}$$

In Eq. 1, n_i, the number of moles of the i-th species in the oven, is given by

$$n_i = \frac{J_i}{\varepsilon_i * T_i * S_s} \quad , \tag{2}$$

where J_i is the detector ion current for the i-th species, ε_i is the ionization efficiency of the RGA ionizer for the i-th species, T_i is the transmission of the RGA quadrupole lens for the i-th species and S_s is the sensitivity of the RGA for a standard gas, given by $S_s = J_s/n_s$. See Refs. 10 and 11 for a more thorough discussion of Eq. 2 and the conditions under which it is applicable.

The transmission through the quadrupole, T_i, is typically constant for $m/q<50$ but decreases at the rate of one decade per 150 AMU beyond there. The precise dependence of T_i on mass differs for each RGA and must be accurately measured if highly quantitative results are required. However, since in our experiments all major measured constituents are at m/q of less than 30, our assumption of a constant quadrupole transmission to the m/q value of 50 will not introduce appreciable error in the use of Eq. 1. The ionization of gases prior to their entry into the quadrupole lens is accomplished in all RGAs by essentially the same technique of flooding the gases with an extended electron beam of about 70 electron volts. Consequently, the ionization efficiencies in Eq. 2 are well known for all species and are obtained from the literature.[12,13,14,15] The sensitivity factor, S_s, is dependent on the geometry of the manifold system from the furnace to the RGA. However, since it is a constant, the determination of mole fractions of individual species, as done by Eq. 1, is independent of it.

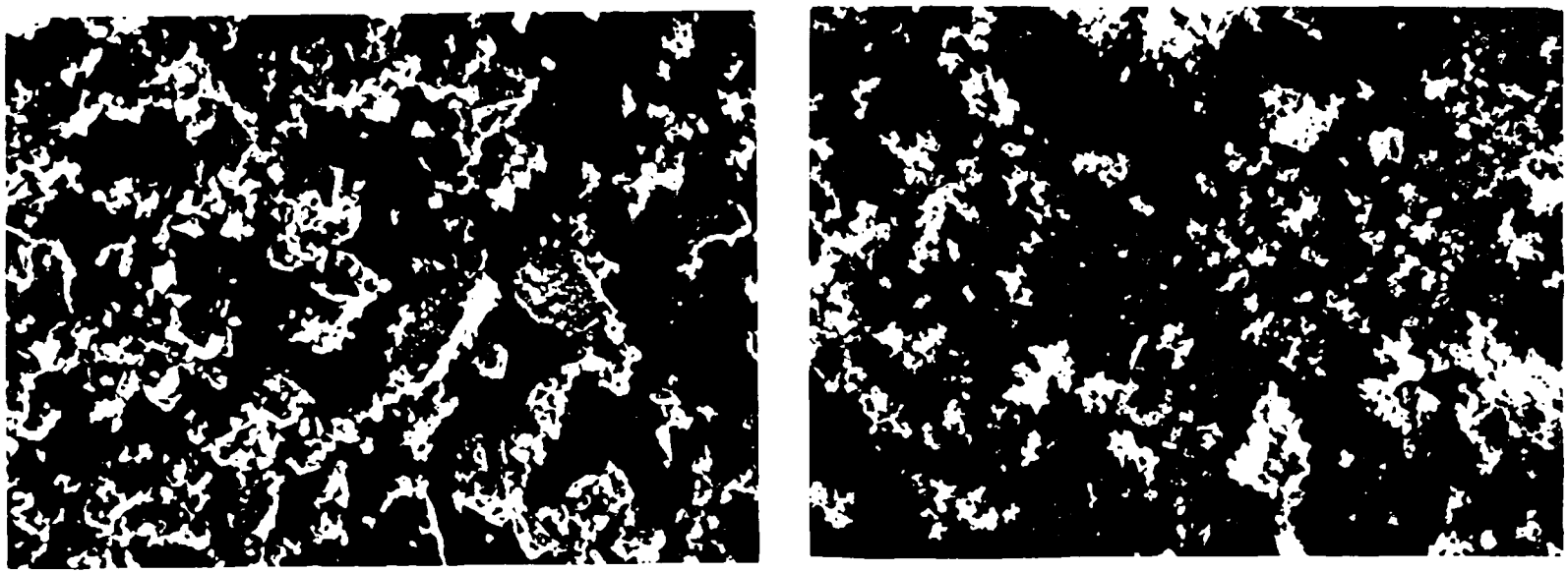

Figure 10. Scanning Electron Micrographs of the boron starting powders with CA Bc powder shown in 10a and CA Ba powder in 10b. Note that the amorphous boron has more fines than the crystalline boron.

The action of the ionizing electrons also causes the gas molecules to break into several m/q fragments. These fragment patterns, more commonly known as cracking patterns, are unique for each species entering the RGA analyzer and are tabulated by several authors.[10,16,17] A careful intercomparison of all observed cracking patterns can result in an accurate identification of the gas species present. For example, CO^+ and N_2^+ both appear at m/q=28. In order to distinguish which species the m/q=28 peak is due to, one must look at possible peaks at m/q of 12, 14 and 16 also. A CO^+ would be accompanied by peaks at m/q of 12 and 16 due to its break-up into C^+ and O^+. In contrast, N_2^+ would be accompanied by N^+ at m/q=14. However, without the use of sophisticated deconvolution methods for RGA spectra,[18] quantitative results for the true gas composition are only approximate for cases where more than one species can contribute to a given m/q value. Consequently, in the data analysis, to avoid erroneous identification by reporting parent species only, all m/q fragments were treated as individual species.

Equation 1 holds true if the relative composition of gases in the RGA ionizer region stays constant over the time period required for the analyzer to sweep through its mass range. In our case, this condition is not strictly true because the composition in the furnace can change during the 5 minute sweep time (see Fig. 3). In addition, the diffusion pump used on the RGA pumps the different species at different rates. Both of these effects will introduce a relative error in the reported mole fractions which is proportional to the m/q difference between the species. However, as our focus of interest lies in the m/q<30 region, this effect does not seriously affect our discussion or conclusions. Unfortunately, because we have not actually made the necessary calibration measurements, the expected uncertainty on our reported mole fractions is impossible to estimate accurately.

In addition to determining the mole fractions of different species present in a given powder, it is also important to measure the relative amount of total volatiles present in different powders. The sensitivity factor, S_s, was the same in measurements with all powders since all were done in identical geometries and RGA conditions. Thus the quantity, M_p, the relative amount of total volatiles present on a powder p, is given by

$$M_p = \Sigma [n_i * S_s] = \Sigma \left[\frac{J_i}{\varepsilon_i} * T_i\right] \quad . \tag{3}$$

Tables 2 through 7 list both the mole fraction, X_i, as well as M_p for each of the powders examined.

Tables 2 and 3 summarize the results for the CA graphite and AE titanium powders respectively. There is very little hydrogen on the graphite but both H^+ and H_2^+ are found in relatively large quantities on the titanium. The H_2^+ is from the TiH_2 layer on the titanium powder because all of it is evolved near 400C, the TiH_2 dissociation temperature (see Fig. 5).

TABLE 2

Gas Species Evolved from CA Graphite

M/q	Species	Mole Fraction
1	H^+	.01
12	C^+	.03
13	CH^+	Trace
14	N^+, CH_2^+	.01
15	CH_3^+	.02
16	O^+, CH_4^+	.05
17	OH^+	.04
18	H_2O^+	.11
25	C_2H^+	.01
26	$C_2H_2^+$	.01
27	$C_2H_3^+$	.03
28	CO^+, N_2^+, $C_2H_4^+$	.56
29	$C_2H_5^+$	.02
30	$C_2H_6^+$	Trace
39	$C_3H_3^+$	Trace
41	$C_3H_5^+$	.01
42	$C_3H_6^+$	.01
43	$C_3H_7^+$	.01
44	CO_2^+, $C_3H_8^+$	.08

Total volatiles, M_p = 7.

The H+ is from water vapor as well as the breakup of H_2^+. Water vapor, indicated by (m/q) values of 18, 17 and 16, is significant for both powders, but it is readily removed by the bakeout process as can be seen from Fig. 4. The absence of a peak at m/q=32, or free oxygen, is indicative that none of the TiO_2 that is bound on the titanium powder is dissociated at these baking temperatures. Ordinarily, TiO_2 is a very stable molecule and its direct dissociation is thermodynamically not favored.[19] At elevated temperatures of 2000C, however, TiO_2 will decompose into oxygen and titanium suboxides. The O atoms liberated in the decomposition of TiO_2 would rapidly recombine with titanium or form neutral oxygen molecules. Under normal circumstances, further dissociation of the lower oxides of titanium can only take place with the aid of some reducing agent.[8] In addition to hydrogen and water, there were also peaks at CO^+, m/q=28, and CO_2^+, at m/q=44. The combination of the peaks at m/q=44 and at m/q=28 implies that the peak at m/q=28 is CO^+ rather than N_2^+. The results for the CA graphite show significant amounts of hydrocarbons as well as a large contribution of CO^+ and CO_2^+. For graphite, the temperature profiles for CO^+ and CO_2^+, Fig. 6, show that they both continue to be evolved even at the highest bakeout temperatures of 1000C.

TABLE 3

Gas Species Evolved from AE Titanium

M/q	Species	Mole Fraction
1	H^+	.13
2	H_2^+	.26
16	O^+	.03
17	OH^+	.14
18	H_2O_+	.34
27	$C_2H_3^+$	.01
28	N_2^+, CO^+	.06
44	CO_2^+	.03

Total volatiles, M_p = 6.

Tables 4, 5, 6 and 7 summarize the results for MON C, CA Ti, CA Bc, and CA Ba respectively. The M_p values shown in Tables 2-7 indicate that AE Ti and CA Gr powders are much cleaner than the other powders. As discussed earlier, impurities fall into two categories: those which are introduced during the fabrication process, and those which are introduced and formed during exposure to the atmosphere. For our powders, the first category includes sulfur compounds and hydrocarbons. The second category includes water vapor, hydrogen, hydrocarbons, and boron hydrides.

While titanium and graphite can be synthesized in relatively pure form, carbon black, including MON C, is made by the incomplete combustion of hydrocarbon byproducts produced in the oil industry. These byproducts, such as bituminous coal and tar, contain high concentrations of unburned hydrocarbon and sulfur impurities. Similarly, traces of sulfur remain during the manufacture of boron powder. These impurities are solid under normal circumstances but readily volatilize during heating. Other hydrocarbon derivatives such as stearates and waxes which are used to improve the flow properties of powders, cannot be easily removed.

Results for MON C, seen in Table 4, show that both the amounts and nature of the evolved gases are different than for CA graphite. First, hydrocarbons are indicated by the presence of the very large amounts of atomic and molecular hydrogen, as well as the series of peaks below m/q of 28 and 16. This combination is not seen for CA graphite in Table 2. The absence of hydrogen for the CA Gr implies that the peak at m/q=28 is predominantly made up of carbon monoxide and molecular nitrogen. For MON C the m/q=28 peak is most likely indicative of a combination of ethylene, C_2H_4, and carbon monoxide. Second, the lower purity of the MON C powder is reflected by the larger M_p figure which indicates a greater amount of gas evolved during baking. Finally, MON C shows the evolution of several sulfur based volatiles which are not seen on CA graphite. The evolution of sulfur monoxide, SO^+ (m/q=48), and sulfur dioxide, SO_2^+ (m/q=64), peaks at a temperature of 200C and then declines slowly until the temperature reaches 600C. The evolution of hydrogen sulfide, H_2S^+ (m/q=34), and carbon disulfide, CS_2^+ (m/q=76), is maximum at a temperature of 300C and is still detected at 800C. However, most of the sulfur based impurities can be eliminated by careful vacuum outgassing at a temperature of 500C. Although their presence remains significant, the measured amounts are much smaller than the corresponding amounts of water vapor, hydrogen, and hydrocarbons.

The evolved gases from the CA Ti are similar in nature to those found for AE Ti with the results summarized in Table 5. Species that are readily identified include hydrogen, water vapor, carbon monoxide, and hydrocarbons. Although, the mole fractions of hydrogen and water vapor are similar for both powders, the total amount of gas liberated for CA Ti is considerably greater than for AE Ti. Another significant difference between the powders is that there are more peaks from hydrocarbon fragments on CA Ti than on AE Ti. Temperature profiles for hydrocarbons indicate that most of them can be removed at 300C. The differences between these Ti powders are consistent with the fact that the CA Ti has a much larger surface area than the AE Ti (See Fig. 9).

TABLE 4

Gas Species Evolved from MON Carbon

M/q	Species	Mole Fraction
1	H^+	.09
2	H_2^+	.21
12	C^+	.02
13	CH^+	Trace
14	CH_2^+	.01
15	CH_3^+	.01
16	O^+, CH_4^+	.04
17	OH^+	.11
18	H_2O^+	.23
25	C_2H^+	Trace
26	$C_2H_2^+$	Trace
27	$C_2H_3^+$	.01
28	CO^+, N_2^+, $C_2H_4^+$	.18
29	$C_2H_5^+$	Trace
32	S^+, O_2^+	.02
33	HS^+	Trace
34	H_2S^+	.01
40	$C_3H_4^+$	Trace
41	$C_3H_5^+$	Trace
42	$C_3H_6^+$	Trace
43	$C_3H_7^+$	.01
44	CO_2^+, CS^+, $C_3H_8^+$	.03
48	SO^+	Trace
64	SO_2^+, S_2^+	.01
76	CS_2^+	Trace

Total volatiles, M_p = 390.

TABLE 5

Gas Species Evolved from CA Titanium

M/q	Species	Mole Fraction
1	H^+	.15
2	H_2^+	.22
12	C^+	.01
14	N^+, CH_2^+	Trace
15	CH_3^+	.01
16	O^+, CH_4^+	.03
17	OH^+	.14
18	H_2O^+	.32
25	C_2H^+	Trace
26	$C_2H_2^+$	.01
27	$C_2H_3^+$	.01
28	CO^+, N_2^+, $C_2H_4^+$	.08
29	$C_2H_5^+$	.01
30	$C_2H_6^+$	Trace
40	$C_3H_4^+$	Trace
41	$C_3H_5^+$	.01
42	$C_3H_6^+$	Trace
43	$C_3H_7^+$	.01
44	CO_2^+, $C_3H_8^+$	.01

Total volatiles, M_p = 20.

TABLE 6

Gas Species Evolved from CA Crystalline Boron

M/q	Species	Mole Fraction
1	H^+	.03
2	H_2^+	.19
12	BH^+, C^+	.01
13	BH_2^+, CH^+	Trace
14	BH_3^+, CH_2^+, N^+	.01
15	BH_4^+, CH_3^+	.01
16	O^+, BH_5^+, CH_4^+	.03
17	OH^+	.11
18	H_2O^+	.34
24	$B_2H_2^+$, C_2^+	Trace
25	$B_2H_3^+$, C_2H^+	Trace
26	$B_2H_4^+$, $C_2H_2^+$	.01
27	$B_2H_5^+$, $C_2H_3^+$	.01
28	$B_2H_6^+$, CO^+, N_2^+, $C_2H_4^+$	.14
29	$B_2H_7^+$, $C_2H_5^+$	.01
32	S^+, O_2^+	.02
33	HS^+	Trace
34	H_2S^+	Trace
40	$C_3H_4^+$	Trace
41	$C_3H_5^+$	Trace
42	$C_3H_6^+$	Trace
43	$C_3H_7^+$	Trace
44	CO_2^+, CS^+, $C_3H_8^+$	.03
48	SO^+	Trace
64	SO_2^+	.03
76	CS_2^+	Trace

Total volatiles, M_p = 18.

TABLE 7

Gas Species Evolved from CA Amorphous Boron

M/q	Species	Mole Fraction
1	H^+	.22
2	H_2^+	.71
3	H_3^+	.02
14	BH_3^+, N^+	Trace
15	BH_4^+	Trace
16	BH_5^+, O^+	.01
17	OH^+	Trace
18	H_2O^+	.01
28	$B_2H_6^+$, CO^+	.01
44	CO_2^+	Trace

Total volatiles, M_p = 3700.

Both crystalline and amorphous boron were tested in the bakeout apparatus. Because of the hygroscopic nature of boron, these powders have significantly lower purity. The CA Bc powder tested, see Table 6, shows many different species. In addition to major impurities such as water vapor, hydrogen, carbon monoxide, and carbon dioxide, there are significant amounts of sulfur impurities, hydrocarbons, and boranes. Most of the water vapor, (m/q=18), evolves at or below 200C for the titanium powders. However, similar to carbon black, the water contamination for boron is so great that trace quantities are still detected at 600C. The evolution of hydrogen, (m/q=2), is peaked in the temperature range of 600-800C indicating that the major sources of hydrogen are the boron hydrides, or boranes B_2H_6 and B_4H_{10}. The evolution of sulfur compounds, SO^+, SO_2^+, H_2S^+ and CS_2^+ continues up to 600C with a maximum level at 400C. The species at m/q=28, believed to be carbon monoxide, evolves at about the same rate throughout the entire temperature range.

As seen in Table 1, the purity of CA Ba is much lower than any of the other powders measured. This fact is confirmed by the large M_p figure in Table 7. Peaks identified were due to hydrogen (H^+, H_2^+, H_3^+), water vapor,

and boranes. Because of the extremely large volume of hydrogen liberated, Table 7 only gives the mole fractions for hydrogen, water vapor and the largest borane peaks. Though not shown, lesser borane peaks appear at m/q=12, 13, [illegible], [illegible], and [illegible]. It may be noted that the large number of peaks from boranes can easily be confused with peaks from hydrocarbons which generally appear in the same m/q range. Therefore, while it is suspected these peaks are predominantly due to boron hydrides, a more careful analysis is required to establish the presence of hydrocarbons.

In order to determine the effect of typical laboratory handling on the impurity content of the powders, four of the powders were baked at 200C. The AE titanium and CA graphite had been handled on a routine basis in the laboratory for several months. That is, the shipping containers were opened in air in order to remove powders for the various experiments, but the cover was replaced tightly each time. The CA Ti2 and CE graphite powders were kept in factory sealed containers until this particular experiment. Then the small amount of powder was removed under argon atmosphere and the powder was immediately placed in the vacuum furnace and pumped down. Each of these powders was baked under vacuum until the pressure stabilized at the system's lower limit of 10^{-6} torr after the bakeout the sample was removed from the furnace and weighed. The results are summarized in Table 8. Weight losses from the samples not exposed in the laboratory environment were within or close to the manufacturer's specifications of their stated purity of the powders. The weight loss from powders not stored under argon in the laboratory was roughly 1.0 percent, somewhat larger than the impurity stated by the manufacturer.

TABLE 8

Powder Impurity from Laboratory Handling

POWDER	% MASS LOSS	% IMPURITY MFR. SPEC.
CA Ti2	.500	1.0
AE Ti*	.790	0.3
CA Gr*	.930	<1.0
CE Gr	.160	0.1

* Exposed to lab environment.

In addition to the 200C bakeouts that tested mainly for water content, the CA crystalline boron powder was baked to 1000C, allowed to cool, removed from the furnace and weighed. Subsequently, it was allowed to sit in the open laboratory environment for several days while its weight gain was monitored. The time history of weight gain is shown in Table 9. During the high temperature bakeout, the powder lost 5.4% of its original weight. Within a few hours

after removal from the oven, the powder had regained about 40% of the weight it had lost, but from then on, the additional gain was quite slow. Though not particularly precise, the implication of this rapid gain in weight is that a large fraction of the impurities is in a predominantly physisorbed state, i.e. relatively weakly bound to the surface such as would be the case with water vapor. These experiments have also demonstrated the extent to which powders shipped from the manufacturer will not retain their guaranteed purity if they are not stored and handled in a moisture free, inert environment.

TABLE 9

Thermogravimetry of CA Crystalline Boron Powder

TIME IN AIR [minutes]	POWDER MASS [g]	% CHANGE
before baking	0.5461	0.00
after baking	0.5164	- 5.44
0	0.5164	0.00
9	0.5206	0.77
109	0.5276	2.05
302	0.5287	2.25
430	0.5292	2.35

3.3 Non-condensible Impurities from the SHS Reaction. The basic assumptions made in the analysis of the RGA data obtained from the reacting samples are threefold. Firstly, the presence of argon in the reaction chamber does not have a significant effect on the SHS reaction or the gas release. This assumption should be quite reliable in that the argon partial pressure is not very high (1 torr) nor can it be expected to undergo chemical reaction with any of the other materials involved. Secondly, the total gas content in the collection bottle remains constant during an RGA scan. This assumption is also reasonably good in that the pressure in the bottle changes by only 7% during one scan of the RGA which takes 5 minutes. Finally, it is assumed that the relative partial pressures of all the species in the bottle remain constant during a scan. This assumption is violated since the pumping speed of any individual species depends on its mass ($v \propto m^{-1/2}$).

Using Eq. 2, it can be shown that the number of moles of a given species in the collection bottle is given by

$$n_i = \left[\frac{J_i}{J_{Ar}}\right] * \left[\frac{\varepsilon_{Ar}}{\varepsilon_i}\right] * \left[\frac{T_{Ar}}{T_i}\right] * n_{Ar} \quad , \tag{4}$$

where all symbols are defined the same as in Eq. 2. As can be seen from Tables 10 and 11, the impurity gases ejected during the reaction consist of free hydrogen, carbon monoxide, free oxygen, carbon dioxide and hydrocarbons. For clarity, the contribution from the argon gas has been substracted out.

TABLE 10

Gas Species From TiC Reaction
Green Compact Not Outgassed Prior to Ignition

M/q	Species	# Moles ($X10^{-6}$)	Mole Fraction
1	H^+	100.	.06
2	H_2^+	700.	.43
3	H_3^+	4.	Trace
12	C^+	11.	.01
13	CH^+	5.	Trace
14	CH_2^+, N^+	39.	.02
15	CH_3^+	37.	.02
16	O^+, CH_4^+	83.	.05
17	OH^+	27.	.02
18	H_2O^+	33.	.02
26	$C_2H_2^+$	10.	.01
27	$C_2H_3^+$	14.	.01
28	CO^+, N_2^+, $C_2H_4^+$	480.	.30
29	$C_2H_5^+$	5.	Trace
32	O_2^+	20.	.01
41	$C_3H_5^+$	3.	Trace
44	CO_2^+, $C_3H_8^+$	11.	.01

Our results are in good agreement with other investigations[20,21,22,23,24] that find hydrogen and carbon monoxide as the major contaminant species. The source of these species is almost certainly the impurities on the reactants rather than any synthesis reaction occurring during the SHS process. The hydrogen is from the decomposition of TiH_2 and the oxygen is from the TiO_2 surface layer on the Ti powder. It is important to note that there was no oxygen evolved from the reactants in the vacuum furnace but that a noticeable amount was evolved during the SHS reaction. This is due to the fact that the baking temperatures did not reach the 2000C necessary to dissociate TiO_2, while the

reaction temperature certainly exceeded that figure. Details of the reaction process will be discussed in a later section. The carbon monoxide, carbon dioxide, and hydrocarbons are predominantly from the graphite. Also noteworthy is the fact that very little water vapor was measured because it most likely condensed out on the vacuum chamber surfaces and never reached the collection bottle.

TABLE 11

Gas Species From TiC Reaction
Green Compact Partially Outgassed Prior to Ignition

M/q	Species	# Moles ($X10^{-6}$)	Mole Fraction
1	H^+	22.	.10
2	H_2^+	78.	.38
3	H_3^+	3.	.02
12	C^+	2.	.01
13	CH^+	2.	.01
14	CH_2^+, N^+	2.	.01
15	CH_3^+	3.	.02
16	O^+, CH_4^+	9.	.04
17	OH^+	8.	.04
18	H_2O^+	14.	.07
26	$C_2H_2^+$	2.	.01
27	$C_2H_3^+$	3.	.02
28	CO^+, N_2^+, $C_2H_4^+$	30.	.15
32	O_2^+	5.	.02
44	CO_2^+	2.	.01

3.4 Condensible Impurities from the SHS Reaction.

3.4.1 Results from Scanning Electron Microscopy. The SHS coated aluminum substrates analyzed by scanning electron microscopy reveal two types of particulate structures. The first type consists of extremely uniform and fine soot particles that coat the substrate uniformly. The second type, appearing randomly dispersed with the fine soot, is irregular, similar to the precursor powders that make up the green compact. Examples of these structures are shown in Fig. 11. Figure 11a shows that the size of fine particles is roughly 50 nm, whereas in Fig. 11b the size of the irregular type particles is roughly

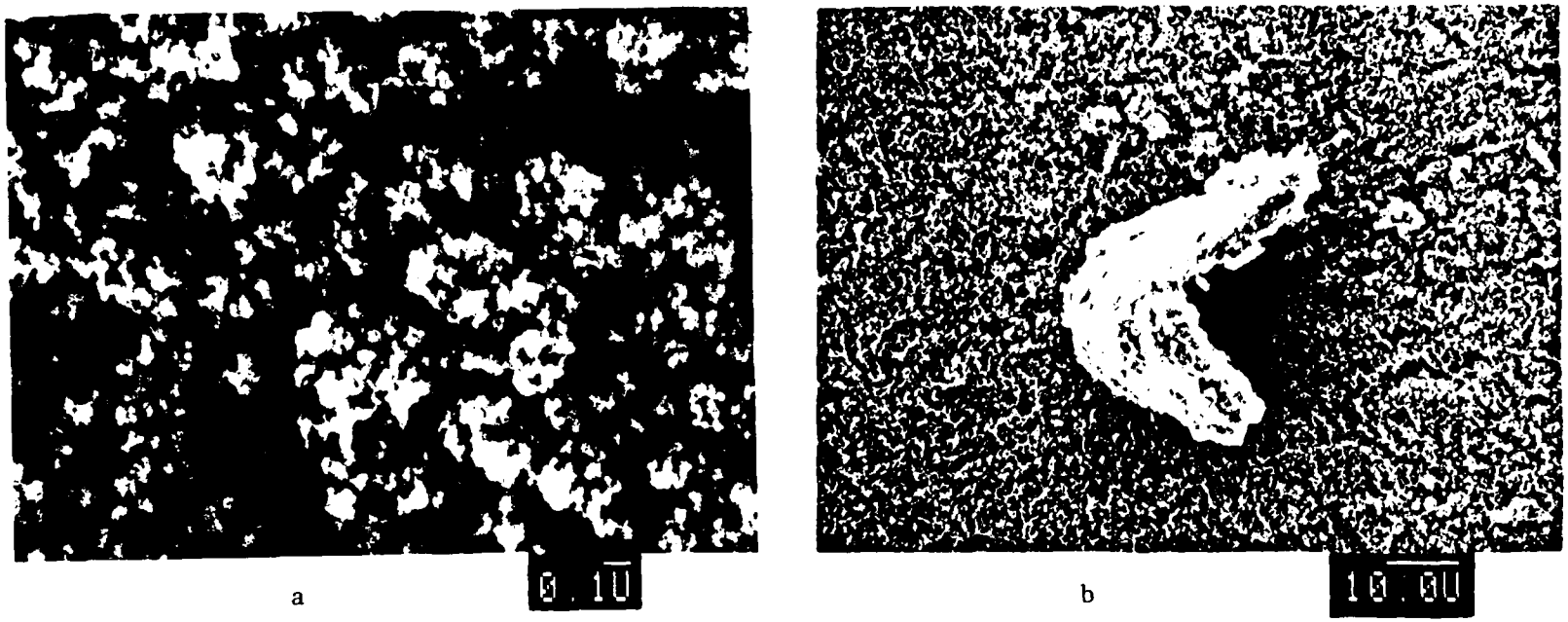

a b

Figure 11. Scanning Electron Micrographs showing substructures of particulates from the TiC reaction. Figure 11a shows the extremely fine soot residue which tends to agglomerate with the individual particles appearing uniformly rounded. Figure 11b shows a particulate which appears to be a chunk of reacted TiC.

10-30 microns. It is speculated that these large irregular particles are really chunks of reacted TiC material that are ejected by the violent gas flow during the reaction. However, the fine soot probably contains unreacted carbon along with the titanium dioxide coating that is released during the reaction.

The impurity coatings obtained in the unbaked and baked reactions are strikingly different. The coating deposited during the unbaked sample reaction is heterogeneous with both the reacted and soot type of particles present, see Fig. 12a. In contrast, the coating deposited during the baked sample reaction is homogeneous and made up of the soot particles only. Furthermore, this coating of submicron soot appears to form very loosely bound micron size nodular aggregate units, see Fig. 12b. Since the characteristics of soot particles in both unbaked and baked coatings seem to be identical, it is believed that the lack of larger reacted particles on the baked sample coating is because the SHS reaction in this case is considerably gentler. That is, in the unbaked reaction, the soot ejecta generated by the SHS burn and the simultaneous generation of the reacted particles by forces disrupting the reacting compact cause both types of particles to be deposited onto the substrate. In the reaction with the baked sample, the disruptive forces of evolved gases are not present and only the fine soot is ejected.

3.4.2 Results from Ion Beam Analysis. The Ion Beam Analysis was carried out on the ejecta collected during the burns of unbaked and baked samples. PIXE was used to identify the elements present in the sample so as to guide the analyses with RBS and NRS. Figure 13 shows the fluorescent x-ray spectra for the two samples with the elements sodium, aluminum, silicon, sulfur, chlorine, potassium, calcium, titanium, chromium, manganese, iron, nickel, copper, and tungsten present. The sources of these elements are: tungsten, sodium, sulfur, chlorine, potassium and calcium from the filament used to ignite the samples; titanium from the Ti powder; iron, nickel, copper, manganese and chromium as impurities in the aluminum substrate; silicon and potassium from the mica stage that held the samples; and calcium from the graphite powder. Carbon and oxygen, which RBS and NRS will show are quite abundant, do not appear in these PIXE spectra because x-rays from carbon and oxygen are absorbed totally in the mylar vacuum foil and the beryllium detector foil.

The elements found with PIXE are used in the analysis of the RBS and the NRS data. See Ref. 9 for details of this procedure. In short, the analysis program "PROFILE" is used. This program uses elemental concentrations and their depth profiles to calculate expected RBS and NRS spectra which are then compared to the experimental data. The concentrations which yield an acceptable fit to the data become the absolute values for the elemental distributions on the surface. Figures 14 and 15 show the RBS and NRS fits along with the concentration profiles for the unbaked and baked samples respectively. Due to the fact that K (A=39) and Ca (A=40) are so close in mass, they cannot be resolved by RBS with the consequence that, in the RBS analysis, the sum of K and Ca is reported as Ca. In addition, some of the elements that are seen with PIXE are not used in the RBS/NRS analyses because of their very low concentra-tions as well as difficulty in resolving from other nearby elements. The total concentrations in the surface layers for the major constituents are tabulated in Table 12.

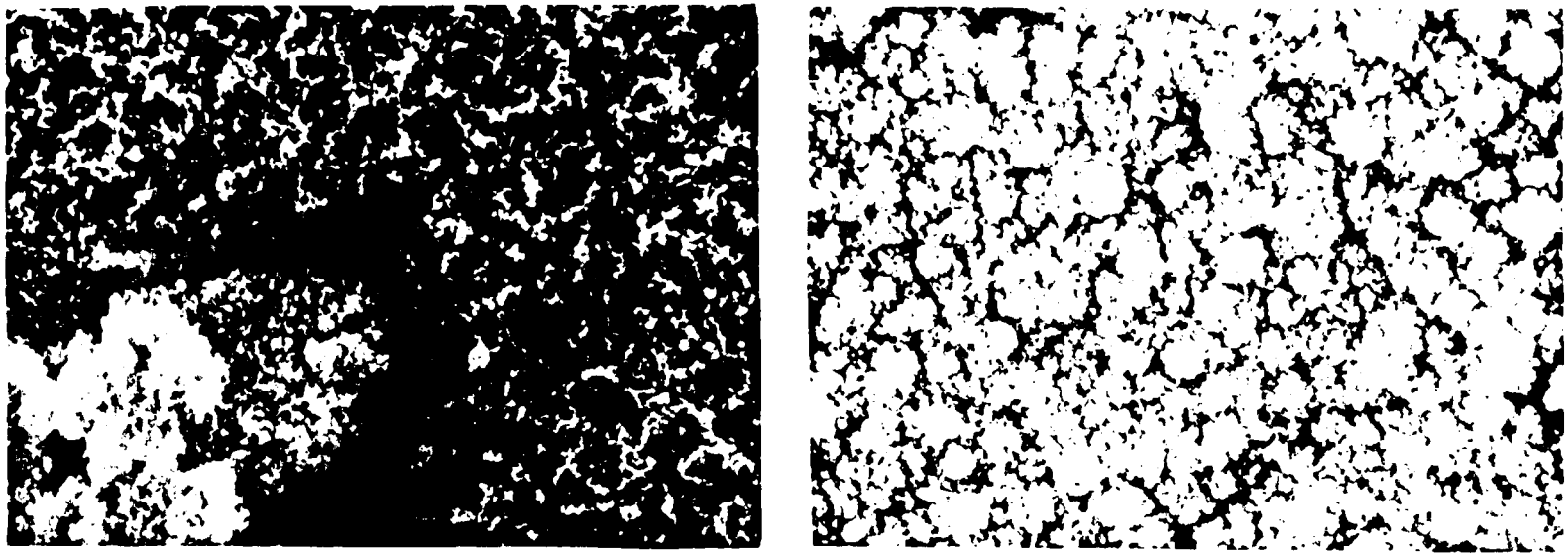

Figure 12. Scanning Electron Micrographs showing the structures of the particulates ejected during the TiC reaction. Figure 12a shows the coating obtained during the reaction of the unbaked sample with both the reacted and sootlike structures evident. Figure 12b shows only the sootlike structure from the reaction from a baked sample.

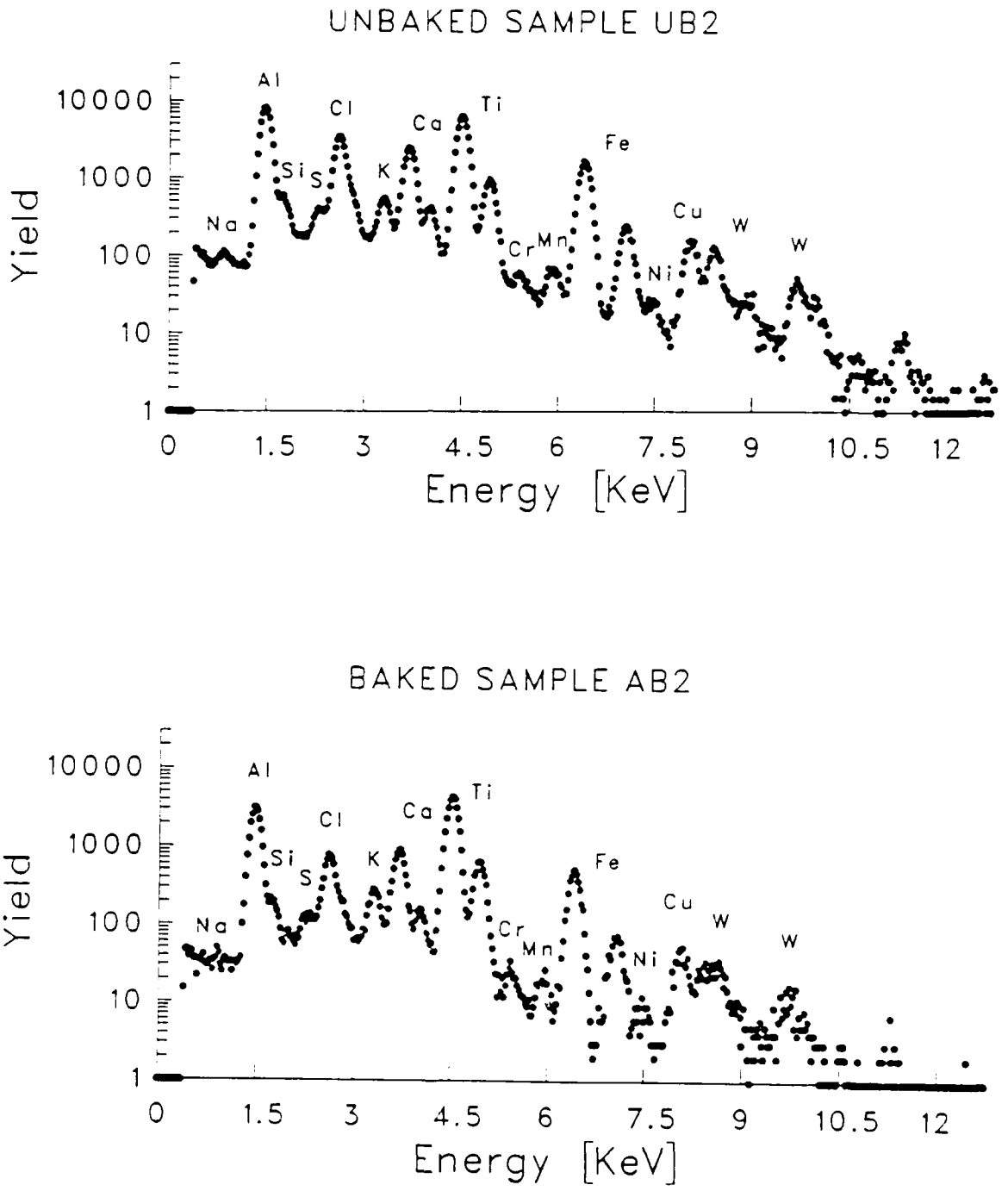

Figure 13. PIXE spectra of the UB2 and AB2 samples.

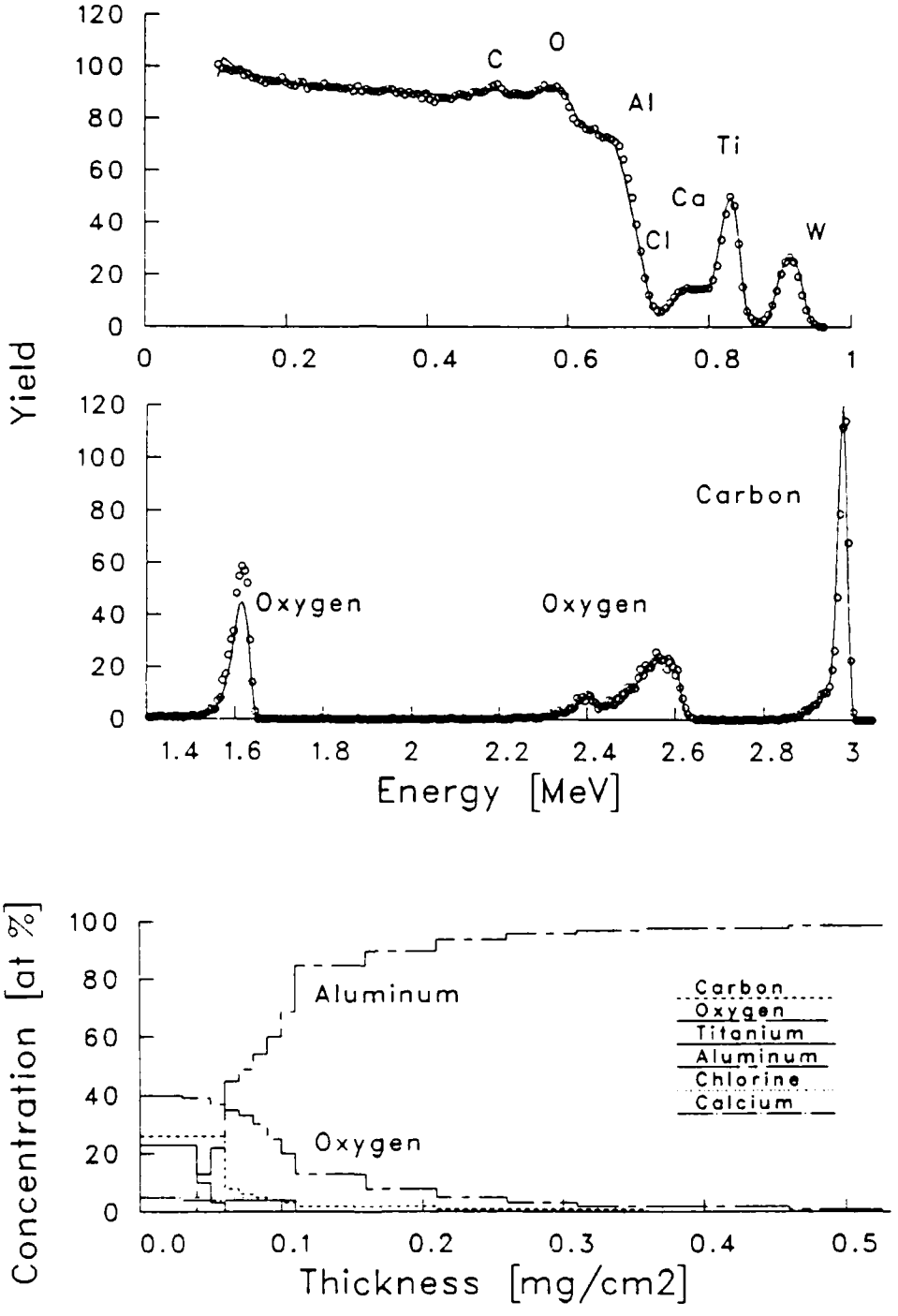

Figure 14. RBS/NRS Results and Elemental Concentration Profiles for the unbaked sample UB2.

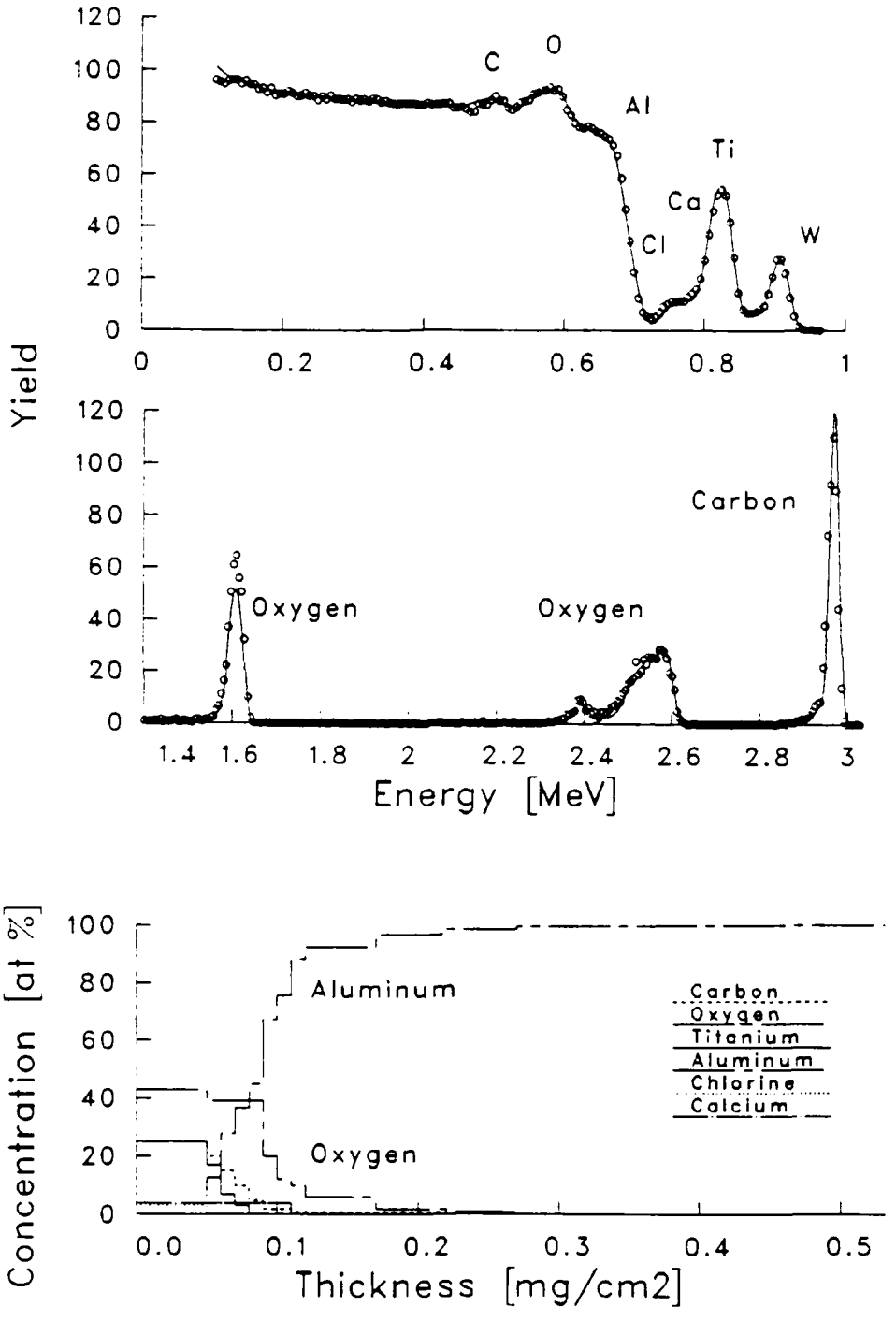

Figure 15. RBS/NRS Results and Elemental Concentration Profiles for the baked sample AB2.

TABLE 12

Elemental Concentrations of SHS Reaction Ejecta

SAMPLE	LAYER THICKNESS [mg/cm^2]	C	O	Ti	Cl	Ca	Fe	W	Al
		[in at/cm^2 x10^{17}]							
AB2	.08	4.1	8.0	3.7	0.6	0.7	0.1	0.1	1.8
UB2	.06	3.8	5.8	2.5	0.8	0.7	0.2	0.1	0.9
AB2	.17	4.4	10.0	3.7	0.9	1.0	0.3	0.2	18.0
UB2	.11	4.4	9.1	2.5	1.3	1.1	0.3	0.2	7.4

As can be seen from Figs. 14 and 15 and Table 12, titanium appears only on the outer layers of the samples while all other elements extend further in with carbon, oxygen and iron being found well into the aluminum substrate areas. The first significant conclusion that can be drawn from this data is that all of the titanium is tied up as TiO_2. The atomic ratios of Ti and O are approximately right for this assignment, with the excess oxygen being tied up as Al_2O_3. One can see that the amount of excess oxygen increases in the deeper layers of the surface, in agreement with the fact that aluminum begins to appear in those deeper layers. If, on the other hand, the assignment of the titanium went to TiC, a possibility which seems in line with the Ti and C concentration numbers, one has to explain the oxygen on the outer surface layers. Since there is no aluminum or none of the other elements in sufficient quantity in these outer layers to bind with the oxygen, and since oxygen cannot remain unbound, the assignment of the oxygen to the titanium is the only possibility. The origin of the TiO_2 is, of course, the oxide layer that is always found on titanium powders. The presence of the carbon can now be attributed to some of the carbon powders in the sample being blown to the aluminum substrate by the action of the volatile gases during the reaction. The fact that the carbon seems to extend quite far into the aluminum (about 3 microns) is indicative of the impurity of the aluminum surface. Figures 14 and 15 show that small quantities of oxygen also extend to these depths.

Another interesting feature about these samples brought to light by the RBS/NRS analysis is the fact that while C, O, Cl, Ca, and Ti are found on the outer surface layers, Fe, W and Al are not. From this information, it is possible to draw additional conclusions about the way in which the ignition and reaction proceeded. The history of what has happened to these samples starts with the very deepest layers and works its way out. The deepest layers contain only Al and Fe in approximately the amount specified for iron impurity for 1010 Aluminum. As layers toward the surface are approached, oxygen and carbon are detected, in agreement with the fact that this aluminum sheet had been exposed to laborabory environments for many years. The cleaning procedure applied is not expected to remove these levels of impurity. The next elements which are observed as the surface is approached are chlorine,

calcium, and tungsten along with a decrease in the amount of aluminum. These features indicate that the tungsten filament has been turned on, but the sample has not yet ignited. The chlorine and calcium are found in the relatively dirty tungsten. Once ignition is achieved, the filament is turned off, explaining why no W or Fe is found on the surface. The Ca and Cl that appear on the surface are most likely due to the fact that they diffuse more readily than the W or Fe.

3.5 SHS Reaction Mechanism and Sample Structures. Investigations of the SHS reaction between the titanium and carbon precursors and their interactions with the oxygen impurity has been extensive. It has been shown[25] that the combustion synthesis reaction between titanium and carbon is actually a liquid - solid reaction where the titanium particle melts, envelops and then reacts with the nearby carbon particles. The interactions between the primary liquid - solid synthesis reaction and the simultaneous generation of large volumes of impurity gases has been studied by several investigators. On one hand, it is suggested that when the titanium particle melts, the oxide surface layer is broken up and carried by the molten Ti phase into the combustion zone.[26,27] There the violent gas evolution and extreme heat of the SHS reaction force these submicron oxide particles out through the porous ceramic body. The Ion Beam Analysis results confirm this mechanism. On the other hand, other investigators imply that the presence of carbon and impurity oxygen promote the synthesis of carbon monoxide and carbon dioxide.[28,29] Additionally, by the action of carbon at extreme temperatures, titanium oxides can be reduced into titanium suboxides, titanium carbide, or free titanium.[30] The RGA results, showing roughly equal amounts of CO^+ and CO_2^+ evolving both from the precursor powders and the reacting samples, provide evidence that little or no oxidation of the carbon occurs during the reaction.

The reacted TiC samples produced in the condensate collection experiment were examined for both interior microstructure and fracture characteristics. When the unbaked sample was reacted, the violent impurity gas flow caused it to be blown into several fragments. In contrast, the baked sample stayed together in a single piece throughout the reaction. In both cases, the interior microstructure of the reacted TiC bodies consisted of fused TiC grains or bands, individual or partially sintered TiC grains, and unfilled voids. However, as seen in Fig. 16, polished surfaces of the unbaked and baked samples do show some differences in their resultant microstructures. In the figure, the light areas are void free titanium carbide and the darker areas are open pores. The polished surface of the unbaked sample, Fig. 16a, shows TiC bands that with open and interconnected porosity. In contrast, see Fig. 16b, an equivalent region of the baked sample shows larger areas of TiC bands with pores that are somewhat smaller and not as deep as those in the unbaked sample. Knoop hardness measurements, using a 400g load, were made on the baked sample. In several instances, the loosely held grains collapsed beneath the diamond indentor, but other measurements of fully dense areas yielded values at, or above HK 1300. This value approaches the hardness of fully dense TiC produced by other means.[31,32] No successful hardness measurements could be made on the unbaked sample because the grains always collapsed under the indentor.

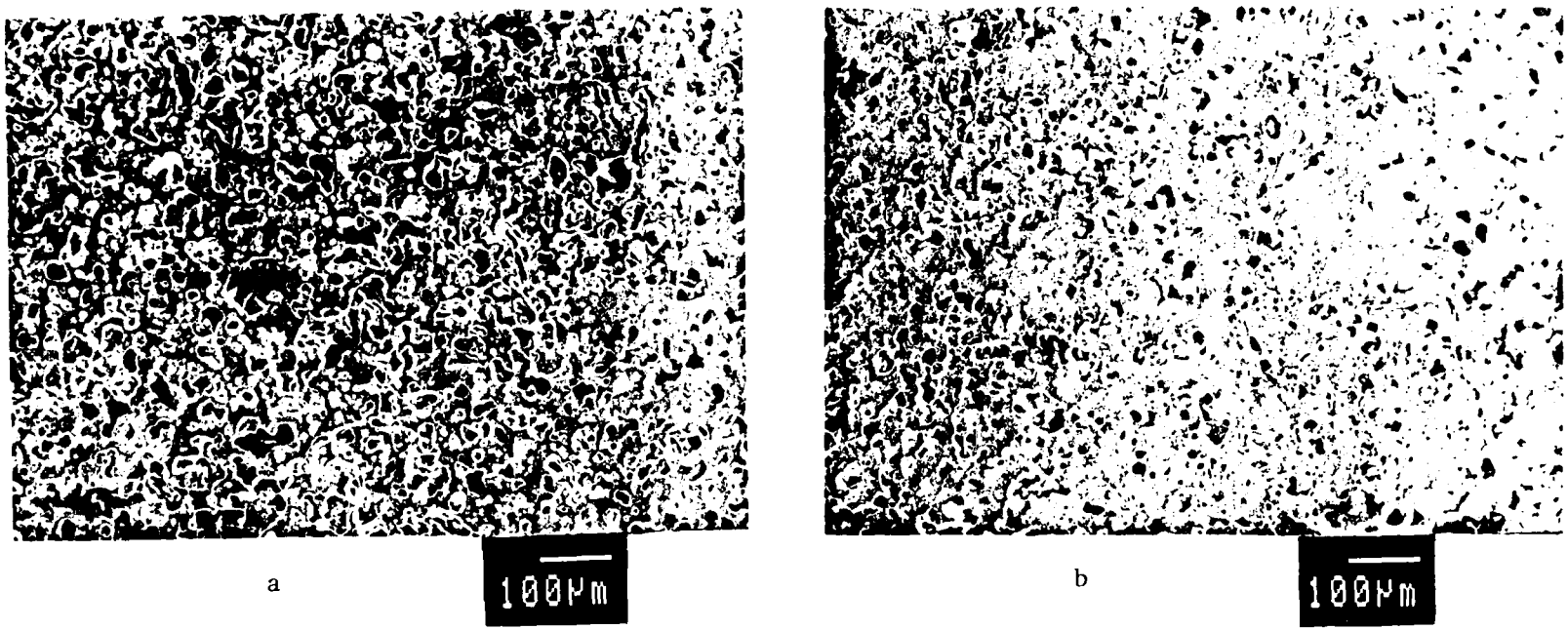

a b

Figure 16. Polished surfaces of the TiC reaction products with 16a showing the unbaked sample and 16b showing the baked sample.

At room temperature, both the unbaked and baked TiC samples failed predominantly by transgranular fracture across the TiC grains with cleavage steps appearing in several grains.[33] As seen in the fractograph of the unbaked sample, Fig. 17a, a few grains also failed by pullouts. In the baked sample, as seen in Fig. 17b, there are more cleavage steps and the pullouts seen in the unbaked sample are absent. While it appears that intergranular bonding in the baked sample is improved, the comparison above indicates only minimal differences. However, examination of pore interiors and the grains lining the pore walls gives a better insight into the failure of these samples. In the unbaked sample the grains lining pore walls are well defined with some sintering present. In the baked sample, however, the grains have sintered to a greater degree, giving an almost melted appearance. In general, the heat generated by the SHS reaction facilitates such post-reaction sintering. However, when the precursors are contaminated with impurities, not all of this heat is available for sintering. Specifically, some heat is lost as the impurity gases are heated to high temperatures and driven out of the reaction zone. As much as 7% of the heat generated by the Ti + C → TiC reaction can go to the heating of the impurity gases found on the precursor powders. Thus, as a result of the greater amount of impurities in the unbaked sample the sintering was less effective than it was in the baked sample. The relatively high hardness values of large TiC grains in the baked sample confirm that the interparticle bonds that result from a greater degree of sintering improve the local strength of the material. Nevertheless, as long as impurities are present, the overall strength of the reaction product will remain poor.

IV. SUMMARY

This experiment has identified several sources of evolving gases from the reactant powders used in the SHS process. The major constituents, in their order of importance, are water vapor which can be driven off at 100C, free hydrogen from the dissociation of TiH_2 at 400 C, free oxygen from the dissociation of TiO_2 at about 2000C, CO, CO_2, and a variety of hydrocarbons. If the SHS reaction is carried out with contaminant laden powders, gross structural defects are produced in the product TiC materials. With these 'dirty' powders, water vapor is boiled off as soon as the compact temperature reaches 100C, followed by the release of hydrogen from TiH_2 at 400C, and CO, CO_2 and hydrocarbons throughout the temperature range. If the combustion wave velocity is fast enough that the impurities cannot evolve out of the sample in the heated region ahead of the front, the very sudden release of volatile vapors at the reaction front is enough to violently disrupt the process.

Several procedures for preventing this structural disruption of the reacting sample have been identified. Most of the hydrogen, water vapor, hydrocarbons and other impurities can be purged in a vacuum oven in several hours at temperatures in the 500C range, thus eliminating much of the potential problem. However, the oxygen released from the TiO_2 cannot be purged at any reasonable bake out temperature. Whenever the powders are vacuum purged, they must then be stored under vacuum or argon until the sample

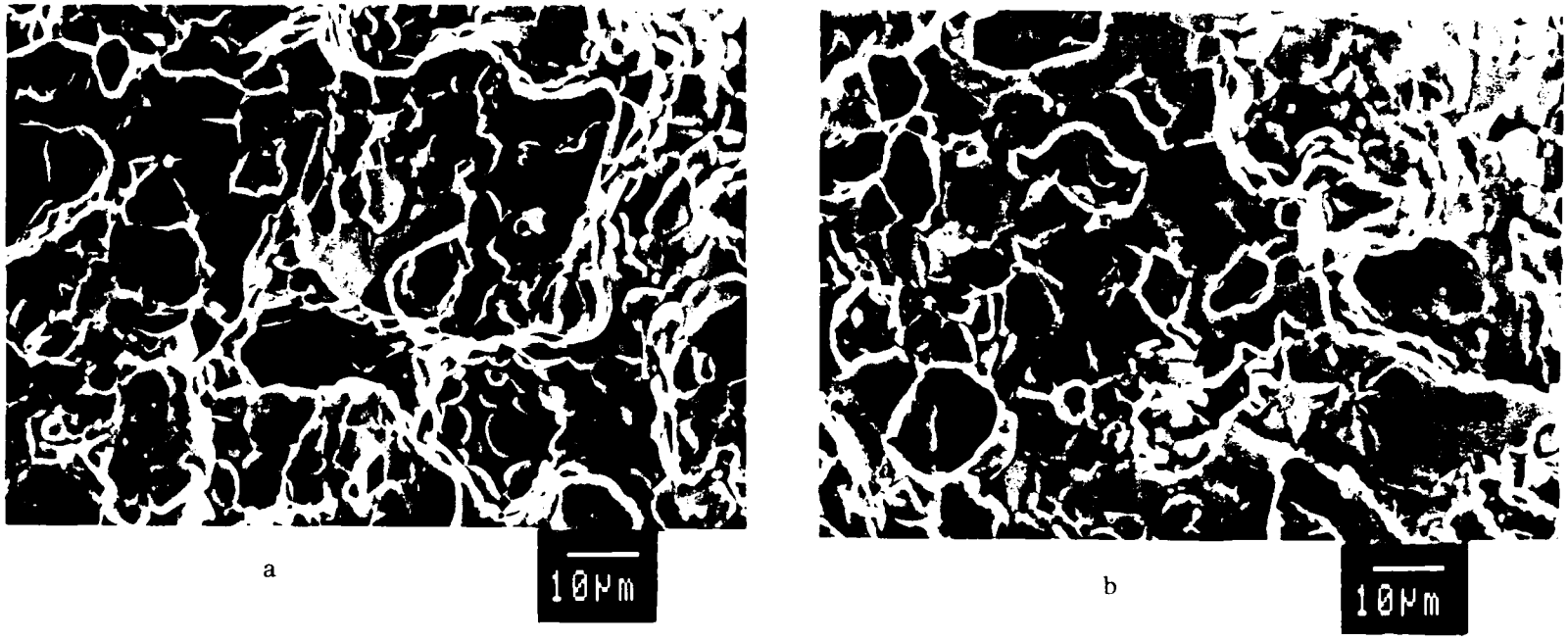

a b

Figure 17. Fractograph of the unbaked and banked samples. 17a shows the fracture surface of the unbaked sample and 17b shows the fracture surface of the baked sample.

is processed. Although it was shown that such storage could be eliminated if the green compact itself is vacuum baked prior to reaction, this procedure itself may not simplify the total processing procedures.

Finally, it cannot be overemphasized that the water vapor, hydrogen and oxygen that we have identified as being major contaminant species are capable of degrading the mechanical properties of ceramics. Thus, until a method is developed which easily and reliably removes these contaminants from reactants to be used in the SHS process, serious problems with structural integrity of the ceramics produced can be expected.

LIST OF REFERENCES

1. System Planning Corporation, Material Fabrication by SHS in the Soviet Union, Vol. II," SPC Report 81-4082, Defense Advanced Research Projects Agency (DARPA), Arlington, VA, December, 1982.

2. Gabriel, K. A. ed., Proceedings of the ARMY/DARPA Symposium on SHS, presented at ARMY/DARPA Symposium, Daytona Beach, FL, November, 1985.

3. Sheppard, L. M., "Powders that Explode Into Materials," Adv. Mater. and Proc., Vol. 130, No. 2, pp. 25-32, February 1986.

4. Henshaw, W. F., Niiler, A., and Leete, T., Self-Propagating High-Temperature Synthesis of Ceramics in Vacuum, ARBRL-MR-03354, Ballistics Research Laboratory, Aberdeen Proving Ground, MD, April, 1984.

5. Holt, J. B., Bianchini, G. M., and Kingman, D. D., Simultaneous Combustion Synthesis and Densification of Refractory Materials, UCRL-93467, Lawrence Livermore National Laboratory, Livermore, CA, January, 1986.

6. Brauer, G., Handbook of Preparative Inorganic Chemistry, Volume 2, Academic Press, New York, NY, 1965.

7. Clark, R. J. H., The Chemistry of Titanium and Vanadium-Preparation Techniques, Elsevier, New York, NY, 1968.

8. McQuillan, A. D., and McQuillan, M. K., Titanium, Butterworths Scientific Publications, London, England, 1956.

9. Niiler, A., Birkmire, R., and Gerrits, J., PROFILE: A General Code for Ion Beam Analysis Spectra, ARBRL-TR-02233, Ballistics Research Laboratory, Aberdeen Proving Ground, MD, April, 1980.

10. O'Hanlon, J. F., A User's Guide to Vacuum Technology, John Wiley & Sons, Inc., New York, NY, 1980.

11. Lin, K., and Burden, J. D., "Mass Spectrometric Solutions to Manufacturing Problems in the Semiconductor Industry," Journal of Vacuum Science and Technology, Vol.15, No. 2, pp. 373-376, March/April 1978.

12. Venugopalan, M., Reactions Under Plasma Conditions, Volume 2, John Wiley & Sons, Inc., New York, NY, 1971.

13. Otvos, J. W., and Stevenson, D. P., "Cross Sections of Molecules for Ionization by Electrons," Journal of the American Chemical Society, Vol. 78, No. 3, pp. 546-551, February 1956.

14. Lampe, F. W., Franklin, J. L., and Field, F. H., "Cross Sections for Ionization by Electrons," Journal of the American Chemical Society, Vol. 79, No. 23, pp. 6129-6132, December 1957.

15. Reed, R. I., Ion Production by Electron Impact, Academic Press, New York, NY, 1962.

16. Drinkwine, M. J., and Lichtman, D., Partial Pressure Analyzers and Analysis, American Vacuum Society, New York, NY, 1979.

17. Stenhagen, E., Abrahamsson, S., and McLafferty, F. W., Registry of Mass Spectral Data, Volume 1, Wiley Interscience, New York, NY, 1974.

18. Dobrozemsky, R., "Experience with a Computer Program for Residual Gas Analyzers," Journal of Vacuum Science Technology, Vol. 9, No. 1, pp. 220-223, January/February 1972.

19. Schick, H. L., Thermodynamics of Certain Refractory Compounds, Volume 1, Academic Press, New York, NY, 1966.

20. Zavitsanos, P. D., and D'Andrea, J. F., Study of Self-Propagating Condensed Phase Reaction-TiB_2 Synthesis, DAAG29-83-C-0017, Army Research Office, Research Triangle Park, NC, February 1985.

21. Holt, J. B., Kingman, D. D., and Bianchini, G. M., "Kinetics of the Combustion Synthesis of TiB_2," Material Science and Engineering, Vol. 71, No. 1-2, pp. 321-327, May 1986.

22. Holt, J. B., and Munir, Z. A., "Combustion Synthesis of Titanium Carbide: Theory and Experiment," Journal of Material Science, Vol. 21, No. 1, pp. 251-259, January 1986.

23. Hansen, G. P., Fredin, L., Margrave, J. L., and Behrens, R. G., Characterization of Vapors Evolved During High-Temperature Synthesis, LA-UR-86-382, Los Alamos National Laboratory, Los Alamos, NM, December, 1986.

24. Fredin, L., Hansen, G. P., Sampson, M. P., Margrave, J. L., and Behrens, R. G., A High-Temperature Quadrupole Mass Spectrometer for Studying Vaporization from Materials Heated by a CO_2 Laser, LA-10744, Los Alamos National Laboratory, Los Alamos, NM, September, 1986.

25. Riley, M. A., and Niiler, A., Low Pressure Compaction of SHS Prepared Ceramics, ARBRL-MR-3574, Ballistics Research Laboratory, Aberdeen Proving Ground, MD, March, 1987.

26. Bloshenko, V. N., Bokii, V. A., and Borovinskaya, I. P., "Dissolution of a Metal Oxide Film During Titanium Carbide Synthesis," Fizika Goreniya i Vzryva, No. 6, Vol. 20, pp. 87-90, November/December 1984.

27. Bloshenko, V. N., Bokii, V. A., Borovinskaya, I. P., and Merzhanov, A. G., "Self-Cleaning of SHS Titanium Carbide from Impurity Oxygen," Fizika Goreniya i Vzryva, No. 6, Vol. 20, pp. 90-94, November/December 1984.

28. Maslov, V. M., Mamyan, S. S., and Voyuev, S. I., "Carbon Interaction with Oxygen During Titanium Carbide Synthesis," Fizika Goreniya i Vzryva, No. 5, Vol. 19, pp. 111-115, September/October 1983.

29. Elizarova, V. A., Rozenband, V. I., Babaitsev, I. V., Gerusova, V. P., and Barzykin, V. V., "Low-Temperature Atmospheric Oxidation of Mixtures of Titanium and Carbon Black or Boron," Fizika Goreniya i Vzryva, No. 1, Vol. 20, pp. 43-48, January/February, 1984.

30. Storms, E. K., The Refractory Carbides, Academic Press, New York, NY, 1967.

31. Miracle, D. B., and Lipsitt, H. A., "Mechanical Properties of Fine Grained Substoichiometric Titanium Carbide," Journal of the American Ceramic Society, Vol. 66, pp. 592-597, August 1983.

32. Toth, L.E., Transition Metal Carbides and Nitrides, Academic Press, New York, NY, 1971.

33. ASM Metals Handbook, Volume 9, ASM Press, Metals Park, OH, 1985.

DISTRIBUTION LIST

No. of Copies	Organization
2	Administrator Defense Technical Info Center ATTN: DTIC-FDAC Cameron Station, Bldg 5 Alexandria, VA 22304-6145
10	C.I.A. OIR/DB/Standard GE47 HQ Washington, DC 20505
1	HQDA ATTN: DAMA-ART-M Washington, DC 20310
1	Commander US Army Material Command ATTN: AMCDRA-ST 5001 Eisenhower Avenue Alexandria, VA 22333-0001
2	Commander U. S. Army Armament Research, Development & Engr Center ATTN: SMCAR-MSI SMCAR-TDC Picatinny Arsenal, NJ 07801-5001
1	Commander Fire Control & Small Caliber Weapons Systems Lab ATTN: DRSMC-SCM Dr. William Ebihara Picatinny Arsenal, NJ 07801-5001
2	Commander U. S. AMCCOM ARDEC CCAC Benet Weapons Laboratory ATTN: SMCAR-CCB-TL Watervliet, NY 12189
1	Commander US Army Armament, Munition and Chemical Command ATTN: AMSMC-IMP-L Rock Island, IL 61299-7300
1	Commander US Army Aviation Systems Command ATTN: AMSAV-ES 4300 Goodfellow Blvd St. Louis, MO 63120-1798
1	Director US Army Aviation Research and Technology Activity Ames Research Center Moffett Field, CA 94035-1099
1	Commander US Army Communication- Electronics Command ATTN: AMSEL-ED Fort Monmouth, NJ 07703-5000
1	Commander US Army Communication- CECOM R&D Technical Library ATTN: AMSEL-IM-L (Reports Section) B.2700 Fort Monmouth, NJ 07703-5000
1	Commander US Army Missile Command Research, Development, and Engineering Center ATTN: AMSMI-R Redstone Arsenal, AL 35898
1	Commander USA Missile & Space Intelligence Center ATTN: AMSMI-YDL Redstone Arsenal, AL 35898-5500
1	Commander US Army Tank Automotive Command ATTN:AMSTA-TSL Warren, MI 48397-5000
1	Director U.S.Army TRADOC Analysis Center ATTN: ATAA-ATOR-TSL White Sands Missile Range NM 88002-5502

No. of Copies	Organization
1	Commandant US Army Infantry School ATTN: ATSH-CD-CS-OR Fort Benning, GA 31905-5400
1	Commander LABCOM ATTN: AMSLC-ASSE 2800 Powder Mill Road Adelphi, MD 20783-1145
1	Commander US Army Development and Employment Agency ATTN: MODE-ORO Fort Lewis, WA 98433-5000
1	Commander US Army Foreign Science and Technical Center ATTN: Mr. Joey F. Crider 220 Seventh Street, NE Charlottesville, VA 22901
5	Commander Army Materials Technology Laboratory ATTN: AMXMR-OM Dr. James W. McCauley Dr. Kenneth Gabriel Ms. Theresa M. Resetar ATTN: AMXMR-MCP Dr. Dennis Viechnicki Watertown, MA 02172
3	Commander US Army Research Office ATTN: Dr. Iqbal Ahmad Dr. Andrew Crowson Dr. Robert Reeber P. O. Box 12211 Res Triangle Park, NC 27709
2	Commander Naval Research Laboratory ATTN: Dr. W. Henshaw, Code 6372 Washington, DC 20234
1	AFWL/SUL Kirtland AFB, NM 87117

No of Copies	Organization
5	AFATL/DOIL (Tech Info Center) Eglin AFB, FL 32542-5438
1	National Bureau of Standards ATTN: D. S. J. Schneider Room A257. Bldg 223 Washington, DC 20234
4	Director Los Alamos National Laboratory ATTN: Dr. R. Behrens, MST-3C348 Dr. Karl F. Wylie, MS G780 Dr. D. Sandstrom, MS-G756 Dr. S. E. Caldwell P. O. Box 1663 Los Alamos, NM 87545
2	Director Lawrence Livermore National Lab ATTN: Dr. J. B. Holt, L-369 Dr. D. Maiden, MS-L71 P. O. Box 808 Livermore, CA 94550
1	Director Sandia National Laboratory Applied Mathematics Div 8231 ATTN: Dr. Stephen B. Margolis Livermore, CA 94550
1	AIRTRON Division ATTN: Dr. John Ings 200 East Hanover Ave. Morris Plains, NJ 07950
1	ALCOA Laboratory ALCOA Tech Center ATTN: Dr. Aaron J. Becker Alcoa Center, PA 15069
1	General Sciences, Inc. ATTN: Dr. P. D. Zavitsanos P. O. Box 185 Norristown, PA 10401
1	Lockheed Palo Alto Research Laboratory ATTN: Dr. Alexander P. Hardt 3251 Hanover Street Palo Alto, CA 94304

No. of Copies | Organization

3 Martin Marietta Laboratories
ATTN: Dr. Dennis C. Nagle
Dr. Stephen R. Winzer
Mr. Michael Riley
1450 South Rolling Road
Baltimore, MD 21227

1 Systems Planning Corp.
ATTN: Mr. William W. Frankhouser
1500 Wilson Blvd.
Arlington, VA 22209

1 Terra Tek, Inc.
ATTN: Raymond A. Cutler
400 Wakara Way
Salt Lake City, UT 84108

2 Defense Advance Research Project Agency
ATTN: Dr. P. A. Parrish
Dr. Gene Farnum
1400 Wilson Blvd.
Arlington, VA 22209

2 Georgia Institute of Tech
ATTN: Ms. Kathryn V. Logan
Dr. Jesse D. Walton
EES/EMSL
Atlanta, GA 30332

1 Rice University
ATTN: Dr. John Margrave
Vice President
Advance Studies Research
P. O. Box 2692
Houston, TX 77252

1 State University of New York
ATTN: Dr. Vladimir Hlavacek
Amherst Campus
Furnas Hall 507
Buffalo, NY 14260

1 University of California
ATTN: Dr. Zuhair Munir
College of Engineering
Davis, CA 95616

Aberdeen Proving Ground

Dir, USAMSSA
ATTN: AMXSY-D
AMXSY-MP, H. Cohen
Cdr, USATECOM
ATTN: AMSTE-SI-F
Cdr, CRDC, AMCCOM
ATTN: SMCCR-RSP-A
SMCCR-MU
SMCCR-SPS-IL

USER EVALUATION SHEET/CHANGE OF ADDRESS

This Laboratory undertakes a continuing effort to improve the quality of the reports it publishes. Your comments/answers to the items/questions below will aid us in our efforts.

1. BRL Report Number_____ Date of Report_____

2. Date Report Received_____

3. Does this report satisfy a need? (Comment on purpose, related project, or other area of interest for which the report will be used.)_____

4. How specifically, is the report being used? (Information source, design data, procedure, source of ideas, etc.)_____

5. Has the information in this report led to any quantitative savings as far as man-hours or dollars saved, operating costs avoided or efficiencies achieved, etc? If so, please elaborate._____

6. General Comments. What do you think should be changed to improve future reports? (Indicate changes to organization, technical content, format, etc.)

CURRENT ADDRESS

Name

Organization

Address

City, State, Zip

7. If indicating a Change of Address or Address Correction, please provide the New or Correct Address in Block 6 above and the Old or Incorrect address below.

OLD ADDRESS

Name

Organization

Address

City, State, Zip

(Remove this sheet, fold as indicated, staple or tape closed, and mail.)

FOLD HERE

Director
US Army Ballistic Research Laboratory
ATTN: DRXBR-OD-ST
Aberdeen Proving Ground, MD 21005-5066

NO POSTAGE
NECESSARY
IF MAILED
IN THE
UNITED STATES

OFFICIAL BUSINESS
PENALTY FOR PRIVATE USE, $300

BUSINESS REPLY MAIL
FIRST CLASS PERMIT NO 12062 WASHINGTON, DC
POSTAGE WILL BE PAID BY DEPARTMENT OF THE ARMY

Director
US Army Ballistic Research Laboratory
ATTN: DRXBR-OD-ST
Aberdeen Proving Ground, MD 21005-9989

FOLD HERE

END
DATED
FILM
8-88
DTIC